Development of an integrated numerical method for the fatigue analysis of railway bogies

by

Brendon Mark Nickerson

Thesis presented in partial fulfilment of the requirements for the degree of Master of Engineering (Mechanical) in the Faculty of Engineering at Stellenbosch University

Supervisor: Prof. G. Venter

March 2017

Declaration

By submitting this thesis electronically, I declare that the entirety of the work contained therein is my own, original work, that I am the sole author thereof (save to the extent explicitly otherwise stated), that reproduction and publication thereof by Stellenbosch University will not infringe any third party rights and that I have not previously in its entirety or in part submitted it for obtaining any qualification.

Date: March 2017

Abstract

Development of an integrated numerical method for the fatigue analysis of railway bogies

B. M. Nickerson

Department of Mechanical and Mechatronic Engineering,
University of Stellenbosch,
Private Bag X1, Matieland 7602, South Africa.

Thesis: MEng (Mech)

March 2017

This study focuses on the creation of a numerical simulation process that can be used to determine the fatigue life of railway bogies, using the Commonwealth railway bogie of the class 5M train in South Africa as example. The numerical simulation is intended for use in future research on railway bogies. The research is supported and funded by the Passenger Rail Agency of South Africa (PRASA) Engineering Research Group at Stellenbosch University. A finite element (FE) model of the bogie has been created using an accurate three dimensional computer aided drawing (CAD) model, supplied by the PRASA Engineering Research Group. The FE model has been used to determine stress distributions due to unit loads applied at the primary and secondary suspension attachment points. Dynamic load cases have been determined through simulation of spring-mass-damper models representing the train and track systems. The load cases have been applied to the FE model stress distributions and superimposed to obtain stress histories. A script has been coded in Python to determine fatigue life from the stress histories. The process has been designed in such a way that each component can be altered and refined, allowing future research opportunities and refinements such as expanding the process to be applied to other bogies or allowing actual measured track data to be used as input for determining dynamic loads. Further research is required to validate and improve the numerical process.

Uittreksel

Ontwikkeling van 'n geïntegreede numeriese metode vir die vermoeidheidsanalise van spoorlyn draaistelle

("Development of an integrated numerical method for the fatigue analysis of railway bogies")

B. M. Nickerson

Departement Meganiese en Megatroniese Ingenieurswese,
Universiteit van Stellenbosch,
Privaatsak X1, Matieland 7602, Suid Afrika.

Tesis: MIng (Meg)

Maart 2017

Hierdie navorsing fokus op die daarstelling van 'n numeriese proses wat gebruik kan word om die vermoeidheidslewe van spoorlyn draaistelle te voorspel. Die "Commonwealth" spoorlyn draaistel van 'n Suid Afrikaans 5M trein word as voorbeeld gebruik. Die navorsing word ondersteun en befonds deur die "Passenger Rail Agency of South Africa (PRASA) Engineering Research Group" by Stellenbosch Universiteit. 'n Eindige element (EE) model van die draaistel was geskep deur die gebruik van 'n akkurate drie dimensionele rekenaargesteunde tekenprogram model, wat deur die PRASA Engineering Research Group verskaf is. Die EE model is gebruik om die verspreiding van die spanning in die draaistel te bereken as gevolg van eenheidslaste op die primêre en sekondêr veringstelsel punte. Dinamiese lasgevalle is deur die gebruik van 'n veer-massa-demper model van die trein en spoor sisteme bepaal. Die lasgevalle is op die EE model se spanningsvelde toegepas en gekombineer om die spanninggeskiedenis te bepaal. Die kode wat hierdie geskiedenis gebruik om die vermoeidheidslewe te voorspel, is in Python geskryf. Die hele proses is ontwerp so dat elke komponent op sy eie verfyn kan word. Dit skep verdere navorsingsgeleenthede soos studies op ander draaistelle of die gebruik van gemete spoor data as inset vir die dinamiese model. Verdere norvorsing is nodig om die proses te verbeter en geldig te maak.

Acknowledgements

Table of Contents

List of Figures

LIST OF FIGURES **viii**

List of Tables

Chapter 1

Introduction

The class 5M train has been in operation in South Africa since 1958. Most of these trains are still in use today, although they have been refurbished and updated (Metrorail, 2007). Some of the challenges currently faced by the rail industry in South Africa are the poor levels of reliability and predictability and the high costs of maintenance due to decades of underinvestment (PRASA, 2014).

One of the most critical structural components of a rail vehicle is the bogie frame. A bogie is a chassis structure used for carrying the wheelsets, attached to the train car body. The design of the bogie used on the 5M train is also known as the Commonwealth bogie. It consists of many components and while some of these are replaced periodically, the cast frames, the mechanical springs and dampers, and the links typically remain intact. Due to the challenging operating conditions experienced, the design life of the bogie is often placed under question.

The importance of bogie fatigue in railway rolling stock has been recognised as a contributing factor in structural failure (Oyan, 1998). This study will focus on the development of methods for use in the prediction of the fatigue life of bogie frames, using the 5M class bogie frame as example.

1.1   Background

The terminology associated with rail vehicles and tracks used in this study is presented in Appendix A.

The structural component most affected by dynamic loads is the bogie frame connected to the wheelsets through the primary suspension and to the car body through the secondary suspension (Luo *et al.*, 1996).

The dynamic loads on the bogie are mostly as a result of track irregularities. These irregularities exist in both vertical and lateral planes affecting track geometry parameters, i.e. unevenness, cross levels, alignment, gauge and twist (Mundrey, 2000). Figure 1.1 shows an example of a vertical track irregularity.
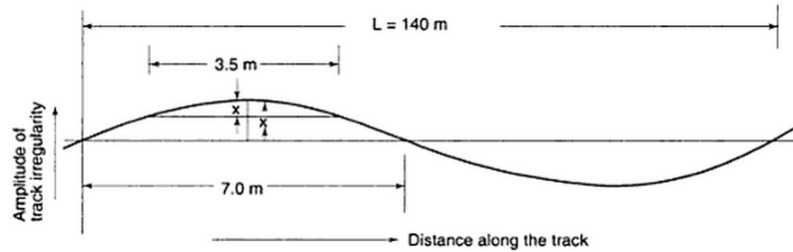
Figure 1.1: Example of a vertical track irregularity (Mundrey, 2000)

For dynamically loaded structures, fatigue life is an important design criterion (Dietz *et al.*, 1998). This is because the dynamic loads result in fluctuating stress magnitudes which can lead to fatigue failure. Thus, bogies need to have a high fatigue resistance to prevent structural failure.

1.2 Objectives

The aim of this study is to design and implement a numerical process that can be used to predict the fatigue life of a bogie frame. The objectives outlined to achieve this aim are:

- To provide a method that determines dynamic loads representing the operating conditions of the bogie;

- To obtain stress histories of the bogie frame due to the dynamic loading;

- To provide a prediction of the fatigue life of the bogie frame based on the obtained stress histories.

1.3 Motivation

This research is funded and supported by the Passenger Rail Agency of South Africa (PRASA).

The current South African rail network includes a number of lines that are poorly maintained and provide less than ideal operating conditions. Furthermore, the rolling stock used by PRASA is often pushed beyond what it is reasonably capable of, with carriages remaining on the line when they should be returning for maintenance. This is partly due to issues with maintenance scheduling, which the PRASA Engineering Research Chair has implemented projects to correct, and partly due to having insufficient rolling stock. Rolling stock is often subject to overloading, especially when delays occur.

It is in this context that this research was initiated by the PRASA Engineering Research Chair, to provide a starting point for predicting whether or not failure will occur. The organisation is interested in the research as it will

later help them predict the remaining life and reliability of bogies currently in service. Knowing the remaining fatigue life of the bogies is important for maintenance, planning for future usage, and evaluating current market value of assets.

The Department of Mechanical and Mechatronic Engineering, Stellenbosch University, has access to Finite Element (FE) software necessary for the completion of the study. An accurate digital 3D model of the bogie was available for use with the software.

The PRASA Engineering Research Chair at the Department of Industrial Engineering, Stellenbosch University, was available to provide assistance and guidance throughout the duration of the study.

Chapter 2

Literature Review

This chapter presents a review of previous research and how it relates to the current study.

2.1 Dynamic analysis

The first objective of this study is to determine the dynamic loads experienced by the vehicle during operation. Specifically the interaction forces at the primary and secondary suspensions that act upon the bogie are needed. This is because these loads are important for the fatigue life prediction of the bogie (Stichel and Knothe, 1998), and they can be used as input for a fatigue strength analysis.

The loads may be defined as recommended by European Standards (EN), International Union of Railways Standards (UIC), or Japanese Industrial Standards (JIS). This approach is generally used during the design process to ensure that components satisfy specifications before they are manufactured and put into service. Mancini and Cera (2006) make use of the EN 13749 standard (BS EN 13749, 2011) and investigates the load cases defined within the standard for use in fatigue failure prediction. They conclude that the use of standards are viable in the design process. However, as the bogie under investigation is already in use, standards such as these will be of limited use. They may be useful as a supplement to load cases determined through other methods.

The loads may also be determined through experimental measurement during operation. Studies such as Ren *et al.* (2011) provide methods to measure the axle spring load, trailing arm seat lateral force and dynamic stresses of bogies. Their study focuses on a 350 km/h electrical-multi-unit (EMU). A similar study could be conducted on the class 5M bogie to measure its operational loads. Another experimental study conducted by Li *et al.* (2015) measures the stress histories of the bogie during experimental operation directly, and these are used to predict the fatigue life. This removes the need for load measurement or prediction altogether.

4

A final way to determine the loads is through simulation. The loads can then be used as is, or even combined with load cases presented by standards to create combined load cases for finite element (FE) analysis. Kim (2006) follows this approach, where the loads obtained through dynamic analysis are combined with load cases from the UIC 615-4 (UIC 615-4, 1994) standard.

For the dynamic simulation of railway vehicles the one approach is to use Multi-body Simulation (MBS) software with track irregularities as input for the simulation to predict the dynamic loads experienced (Stichel and Knothe, 1998), see Figure 2.1. Dietz *et al.* (1998) conducted such a study where the use of commercial MBS software was combined with commercial fatigue life prediction codes.

A major advantage of MBS software is the ability to make requests for various analysis features (Dietz *et al.*, 1998), as depicted in Figure 2.2. In the case of the current research, an inverse dynamic analysis of the bogie could be performed. Inverse dynamics is the calculation of forces and moments by using kinematics and data for mass and moment of inertia, effectively using Newtons second law of motion in reverse (Livingstone, 2008). This would result in dynamic load histories that can be used to construct stress histories of the bogie.
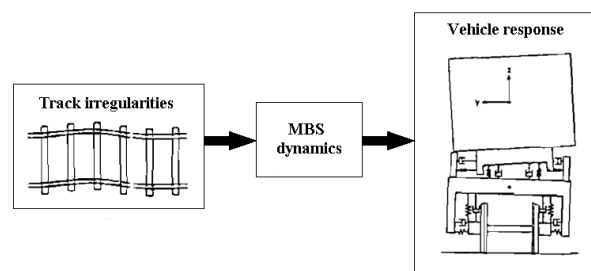
Figure 2.1: Concept of railway dynamic simulation, adapted from Stichel and Knothe (1998)

Due to a general tendency towards lightweight structures, the elastic deformations of the bodies in the MBS can no longer be neglected (Dietz *et al.*, 1998). Small deformations of the bogie can be taken into account by using FE software to generate flexible bodies for use in MBS software. This also allows for the direct simulation of the bogie stress history. The flexible bodies included in the MBS simulation would contain the necessary information to return the strain and stress fields of the body due to the deformation experienced during the simulation.

The use of MBS software is predicated on the availability of commercial software licenses which are often costly. Instead of using MBS software, models
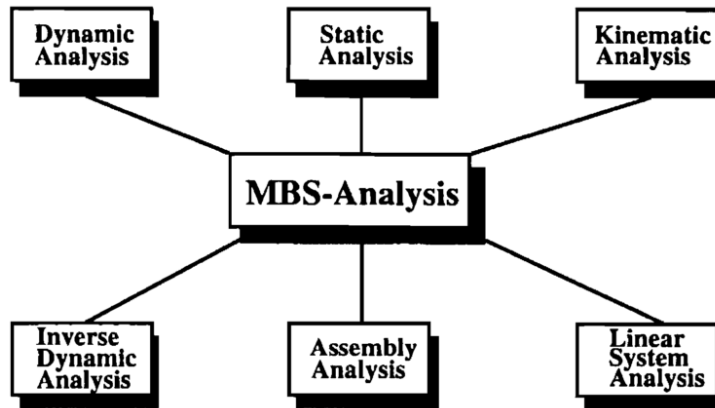
Figure 2.2: MBS-analysis features (Dietz *et al.*, 1998)

representing the dynamic behaviour of systems can be used. These models typically consist of lumped masses connected via dampers and springs.

A number of researchers have opted for the use of such models in their studies. These include Grassie *et al.* (1982), Zhai and Sun (1994), Nielsen and Igeland (1995), Sun and Dhanasekar (2002), and Ferrara *et al.* (2012).

In particular Sun and Dhanasekar (2002) constructed a detailed and validated vehicle-track interaction model that can be used to predict interaction forces between various components. Their model is depicted in Figure 2.3 and consists of a ten degree of freedom vehicle model representing the bounce and pitch of the carriage and bogies and the bounce of the wheelsets, resting in a four layer track model representing the rail, sleepers, ballast and subballast. A model such as theirs can be used to predict the forces at the primary and secondary suspensions due to irregularities modelled on the wheel or rail.

2.2 Fatigue analysis

Once the loads have been determined, a structure can be analysed for its fatigue resistance. Again, this can be done either based on the standards, through experimentation, or through numerical simulation.

A fatigue failure can be defined in stages provided by Budynas and Nisbett (2011). The first stage is the initiation of microcracks due to cyclic plastic strain. These cracks are often not visible to the naked eye. The second stage sees a progression from micro- to macrocracks forming parallel fracture surfaces separated by longitudinal ridges. During loading, these cracked surface repeatedly open and close which causes crack growth. The final stage occurs when the remaining material can no longer support the applied loads and a sudden fracture occurs.

The fatigue life prediction is often conducted using one of three major approaches (Budynas and Nisbett, 2011). These approaches are:
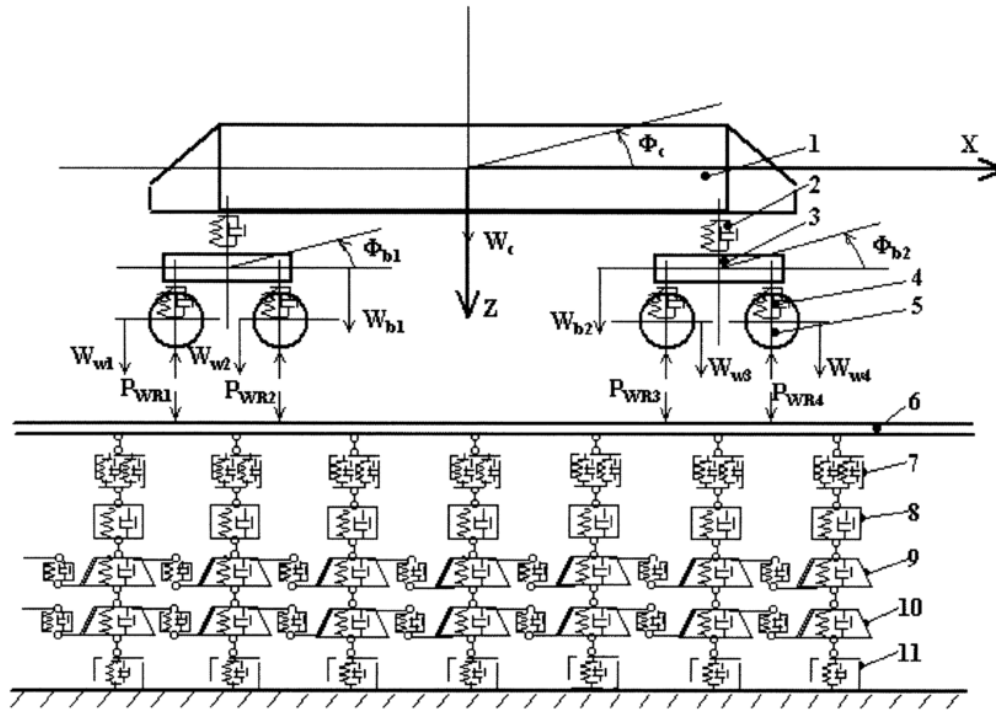
1 – Wagon Body (M_c – mass, J_c – inertial moment),
2 – Secondary Suspension (K_{sc} – stiffness coefficient, C_{sc} – damping coefficient),
3 – Bogie (M_b – mass, J_b – inertial moment),
4 – Primary Suspension (K_{pr} – stiffness coefficient, C_{pr} – damping coefficient),
5 – Wheelset (M_w – mass),
6 – Rail (Timoshenko Beam)
7 – Fastener and Pad (K_f, K_p – stiffness coefficients, C_f, C_p – damping coefficients),
8 – Sleeper (M_s – mass, K_{sl} – stiffness coefficient, C_{sl} – damping coefficient),
9 – Ballast (M_{bl} – mass, K_{bl} – stiffness coefficient, C_{bl} – damping coefficient),
10 – Subballast (M_{sb} – mass, K_{sb} – stiffness coefficient, C_{sb} – damping coefficient),
11 – Subgrade (K_{sg} – stiffness coefficient, C_{sg} – damping coefficient).

Figure 2.3: Dynamic model developed by Sun and Dhanasekar (2002)

- The stress life (S-N) method;

- The strain life (ϵ-N) method;

- And the fracture mechanics method.

The S-N method makes use of experimental material testing on a large number of specimens. The specimens are exposed to repeated cyclic loading at various stress amplitudes and the cycles to failure is counted. An S-N curve is then plotted, which provides the relationship between stress amplitude and cycles to failure for the given material. This method is the most widely utilised due to its ease of use and the large amount of published data available for its use (Budynas and Nisbett, 2011), and is most suited to high cycle fatigue life

prediction. It is, however, generally the least accurate method especially when predicting low cycle fatigue failure.

Where the S-N method only looks at elastic strains, the ϵ-N method takes into account plastic strains that occur when material fails due to fatigue. When fatigue failure occurs, it will often take place at some stress concentration. Should the stress at this location exceed the material's elastic limit then plastic strain will occur which alters the elastic limit of the material. This method is better suited for low cycle fatigue than the S-N method.

The fracture mechanics approach focuses on monitoring crack growth within a material. An initial crack length is assumed or measured and the failure can be assumed by predicting the growth of the crack subject to a given stress cycle. This method is especially useful when a fatigue crack has already been identified and requires analysis.

The majority of researchers in the literature have used the S-N method for the fatigue life prediction of bogies. The reason for this is that the simpler S-N method provides sufficiently accurate predictions for high cycle fatigue, removing the need for using the more complex methods. Furthermore, Dowling (2007) states that for high cycle fatigue lives, where elastic strain dominates, the ϵ-N and S-N based approaches can be considered equivalent. One way of using the S-N method is to consider the endurance limit of the material. The endurance limit method has been the main one used since the issuing of the UIC leaflets (Cera *et al.*, 2008) and it is also used for the analysis of fatigue static tests. In this method the maximum and minimum stresses generated by all the load cases separately applied are determined on each point of the bogie frame (Cera *et al.*, 2008). From these values the mean stress, σ_m, and stress amplitude, σ_a, are defined:

$$\sigma_m = \frac{\sigma_{max} + \sigma_{min}}{2} \tag{2.1}$$

$$\sigma_a = \left| \frac{\sigma_{max} - \sigma_{min}}{2} \right| \tag{2.2}$$

The mean stress and fatigue cycle amplitude can then be compared with the fatigue limit of the material, using some specified failure criterion. Figure 2.4 depicts a number of these failure criteria.

This method is particularly useful to quickly determine whether or not fatigue failure will occur. It is also the method recommended in standards such as EN 13749 for use in the design process. However it cannot predict the number of cycles to failure should it occur. For this to be done, a cumulative damage method needs to be used along with an S-N curve.

Cumulative damage models consider all the effects due to combinations of load cases (Cera *et al.*, 2008). Miner's rule is one of the most simple cumulative damage theories, being a linear damage rule (Fatemi and Yang, 1998). It states
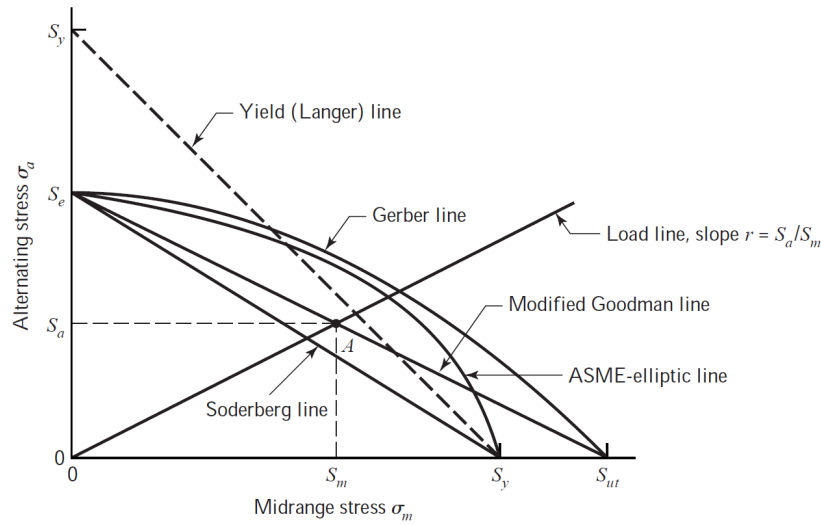
Figure 2.4: Fatigue failure criteria for endurance limit method (Budynas and Nisbett, 2011)

that if there are k different stress levels and the number of cycles to failure at the ith stress level (S_i) is N_i, then:

$$\sum_{i=1}^{k} \frac{n_i}{N_i} = D \tag{2.3}$$

where n_i is the number of cycles accumulated at the stress level S_i and D is the fraction of life used due to the cycles at each stress level. When the damage fraction is equal to 1 then failure is assumed to occur. The cycles to failure can then be determined as the inverse of the damage fraction. The stress level S_i is determined using the σ_a and σ_m of the cycle. The σ_a is first corrected using the cycle's σ_m, in order to obtain the equivalent stress level (S_i) at a zero mean stress. This is necessary as often an S-N curve is obtained using fully reversed loading, where the mean stress is zero, and the effect of the mean stress on the stress amplitude must be taken into account before a comparison with the S-N curve can be made. The corrected amplitude is then compared to the S-N curve to retrieve the value of N_i.

Fatemi and Yang (1998) also study more advanced cumulative damage theories and compare them. They provide a summary of cumulative damage theories from 1945 to 1992, including linear damage rules, nonlinear damage curve and two-stage linearisation approaches, life curve modification methods, crack growth approaches, approaches based on continuum damage mechanics models, and energy based theories.

In order to make use of cumulative damage methods for the fatigue life prediction of a bogie, the stress or load history of the bogie under its operational conditions needs to be determined. This is the second objective of this

study and can be achieved through experimental measurement or numerical simulation.

Dynamic loading experienced by structures will often vary drastically over time and contain cycles at various amplitudes. Therefore cumulative damage models also need to apply cycle counting methods to the stress histories to determine the number of cycles experienced at a given stress amplitude. A number of cycle counting techniques are discussed by Lee *et al.* (2005). A large number of previous researchers, such as Dietz *et al.* (1998), Stichel and Knothe (1998), Luo *et al.* (1998), Han *et al.* (2013), and Li *et al.* (2015), have made use of the rainflow cycle counting method.

In the study conducted by Li *et al.* (2015), stress histories were directly measured at key locations on a Beijing Subway vehicle bogie. These stress histories were then analysed using rainflow cycle counting and the S-N method along with cumulative damage rules. Figure 2.5 shows the process followed in their study. The fatigue analysis of stress histories obtained in this study will be conducted in a similar fashion.
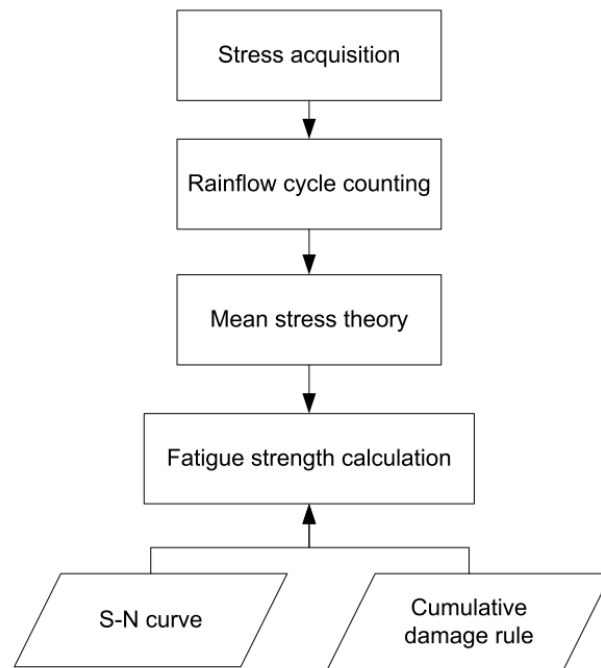
Figure 2.5: Process for fatigue analysis (Li *et al.*, 2015)

Some studies that have made use of numerical simulation include Luo *et al.* (1996), Dietz *et al.* (1998), Stichel and Knothe (1998), Kim (2006), and Han *et al.* (2013). In general, the approach has been the same. FE software has been used to conduct a stress analysis of the bogie and to determine critical points within the structure. These critical points are then further analysed for

fatigue resistance and this is used to predict the fatigue life of the structure. As the Department of Mechanical and Mechatronic Engineering at Stellenbosch University has access to licenses for FE software, this is a promising route for the current study.

A weakness of using FE software lies in the assumptions made for the boundary conditions (Dietz *et al.*, 1998). For static structures the boundary conditions may be defined easily. This is not necessarily so for dynamically loaded structures as is the case with the railway bogie. The time varying boundary and load conditions can be determined using MBS software, which delivers realistic loads for the analysis of stresses and life cycle calculations (Dietz *et al.*, 1998).

Another possibility is to substitute the inertia relief analysis technique Liao (2011) for the use of boundary conditions. This technique allows for the analysis of unconstrained structures by calculating the sum of the forces and moments and applying an equivalent inertial load to force a state of equilibrium. It is available in most commercial FE software packages.

It should be noted that the use of cumulative damage theories is conducted within the time domain. The stress history of the bogie can also be analysed in the frequency domain. Younesian *et al.* (2009) studied these two approaches in their research, comparing cumulative damage to estimate fatigue life in the time domain and estimating fatigue life in the frequency domain. To do this a power spectral density (PSD) of the stress is obtained using FE software. The fatigue life is estimated by applying the Rayleigh technique in random fatigue theory to the PSD. They found that the use of cumulative damage in the time domain lead to more conservative fatigue life estimates. They also show that the frequency domain facilitates simpler analysis of random vibrations. As the dynamic loads in this study will be determined using specifically defined irregularities, the more conservative time domain method will be preferred.

Based on the reviewed literature and considering the resources available for this study, it was decided to make use of a dynamic model to determine operational loads acting on the bogie. Furthermore, the stress histories of the bogie will be determined using an FE model in conjunction with the determined loads and the fatigue analysis will be conducted using the S-N method.

Chapter 3

Outline of the Numerical Simulation Process

The complete numerical simulation process proposed by this study is summarised in Figure 3.1.
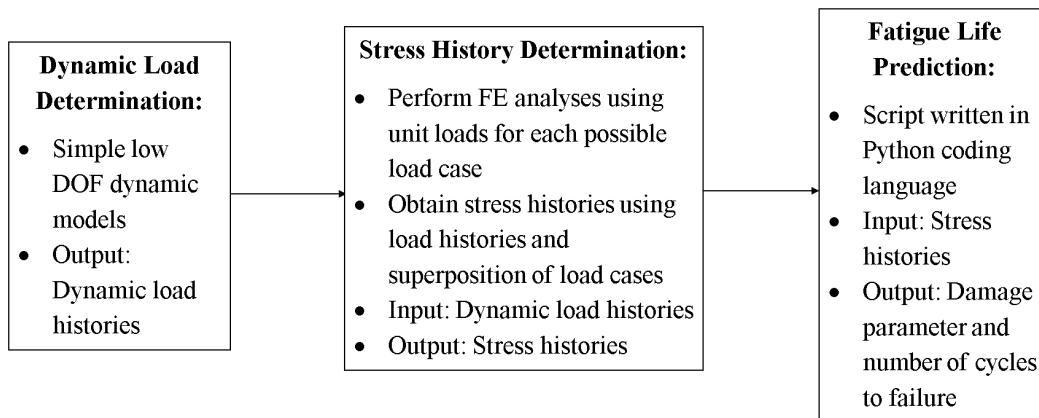
Figure 3.1: Numerical simulation process

The process consists of three separate numerical procedures, each of which is aimed at achieving one of the specified objectives of the study as outlined in Section 1.2.

The dynamic load determination is achieved through a simple rail vehicle-track interaction model, that only simulates vertical track irregularities and the responses caused by them. The model is defined mathematically through the use of Newton's Second Law and equations of motion. The Newmark-β numerical integration scheme is used to solve the model at each time step during simulation. The inputs for the model are taken from literature. Though this will not provide practical results, the results are sufficient to prove that the model performs adequately. The model provides the load histories of the

12

interaction forces at the primary and secondary suspensions as output. The development and validation of the dynamic model is detailed in Chapter 4.

The stress history determination is achieved through the use of FE software combined with the outputs of the dynamic model. A detailed FE model of the class 5M bogie has been constructed and is used to obtain stress fields due to unit loads applied at the primary and secondary suspension attachments. The stress fields due to each unit load are then multiplied by the dynamic load histories of their respective suspension system, and superimposed to obtain stress histories for each element in the FE simulation. The creation of the FE model is detailed in Chapter 5.

The final numerical procedure determines the fatigue life for a given stress history. It takes as input the stress histories determined through use of the FE model. A script has been written using Python based on the S-N method for fatigue life prediction. The script provides a cumulative damage parameter and the number of cycles to failure for the stress history provided for each element in the FE model. These parameters can then be displayed and investigated. The development and validation of the fatigue script is detailed in Chapter 6.

These procedures are designed to be independent of one another and each procedure can receive inputs from or pass outputs to another source. For example, the fatigue life prediction script could receive a stress history determined from experimentally measured strain data as an input.

Finally, these procedures are combined and implemented to determine the fatigue damage experienced by the bogie for a given track irregularity. The integration of the numerical procedures is explained in Chapter 7.

Chapter 4

Dynamic Modelling

This chapter details the development and validation of a numerical dynamic model that can be used to predict the interaction forces at the primary and secondary suspensions of a rail vehicle. These forces represent the operational loading of the bogie as the vehicle travels along a track.

4.1   Description of the dynamic model

The model is based on similar models found in literature reported in Section 2.1. The model is depicted graphically in Figure 4.1
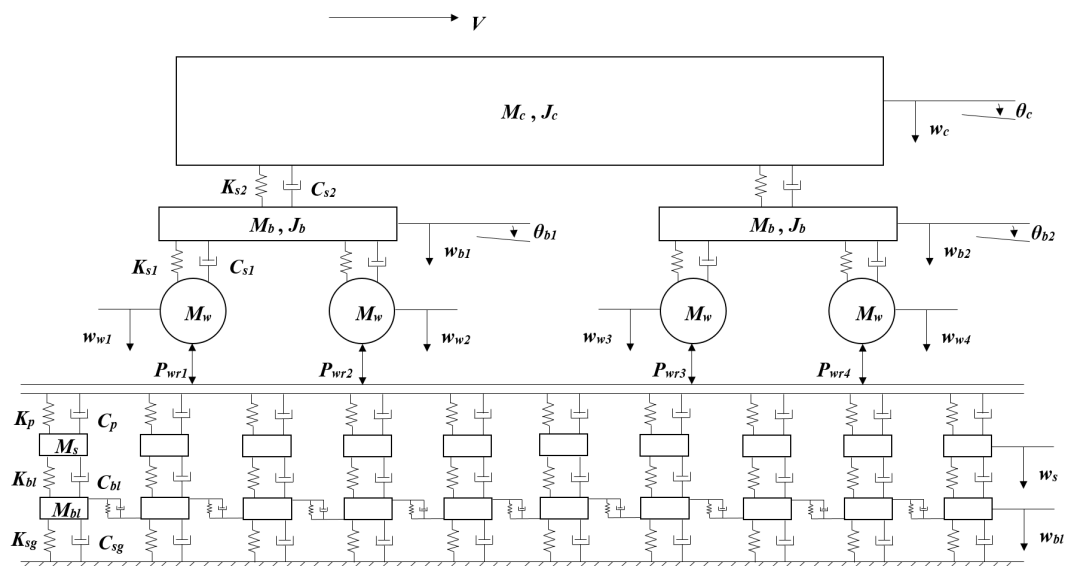
Figure 4.1: Dynamic model for vertical interaction of rail vehicle and track systems

For the model, it is assumed that the responses are symmetric across the vertical plane and thus only half of the system is modelled. This means the

14

model is effectively half a vehicle resting on top of a single rail. The vehicle is assumed to move at a constant speed in the longitudinal direction. Only vertical interactions between and within the vehicle and track components are modelled.

The vehicle system consists of the carriage body, and the leading and trailing bogies each with two wheelsets. The wheelsets are connected to the bogies through the primary suspension, whilst the bogies are connected to the carriage body through the secondary suspension. Both the bounce and pitch of the carriage and bogies are taken into account in the model.

The rail track system is a three layer model. It consists of a discretely supported beam, representing the rail, with ends situated far enough away for the beam to be considered infinitely long. The discrete supports represent the sleepers which rest on the ballast.

4.2 Equations of the dynamic model

The equations used to construct the dynamic model depicted in Figure 4.1 are presented in this section.

4.2.1 Rail vehicle equations of motion

The free body diagram (FBD) of the leading bogie is presented in Figure 4.2.

$$C_{s2}(\dot{w}_c + L_c\theta_c) + K_{s2}(w_c + L_c\theta_c) - C_{s2}\dot{w}_{b2} - K_{s2}w_{b2} + M_bg$$

$$M_b\,,\,J_b$$

$$\theta_{b2}$$

$$w_{b2}$$

$$C_{s1}\dot{w}_{w3} + K_{s1}w_{w3} - C_{s1}\dot{w}_{b2} - K_{s1}w_{b2}$$

$$C_{s1}\dot{w}_{w4} + K_{s1}w_{w4} - C_{s1}\dot{w}_{b2} - K_{s1}w_{b2}$$
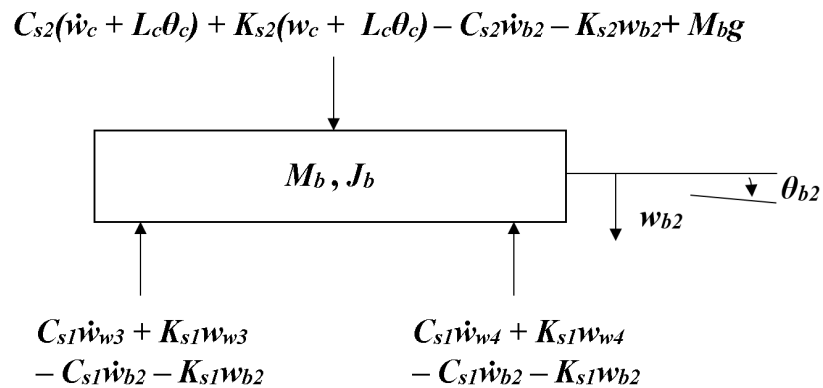
Figure 4.2: Free body diagram of leading bogie

From this FBD the equations of motion for the bogie are derived using Newton's second law, Equation 4.1. This states the sum of forces applied to an object is equal to the product of the mass of the object and its acceleration. Similarly, the sum of moments applied to an object is equal to the product of its mass moment of inertia and its angular acceleration.

$$\Sigma F = m\ddot{x} \tag{4.1a}$$

$$\Sigma M = J\ddot{\theta} \tag{4.1b}$$

The two equations derived for the leading bogie using Equation 4.1 are given below. Equation 4.2 describes the bounce motion of the bogie and Equation 4.3 describes the pitch motion of the bogie.

$$M_{b2}\ddot{w}_{b2} + (C_{s2} + 2C_{s1})\dot{w}_{b2} + (K_{s2} + 2K_{s1})w_{b2} - C_{s2}(\dot{w}_c + L_c\dot{\theta}_c)$$
$$- K_{s2}(w_c + L_c\theta_c) - C_{s1}\dot{w}_{w3} - K_{s1}w_{w3} - C_{s1}\dot{w}_{w4} - K_{s1}w_{w4} = M_b g \tag{4.2}$$

$$J_{b2}\ddot{\theta}_{b2} + 2C_{s1}L_b^2\dot{\theta}_{b2} + 2K_{s1}L_b^2\theta_{b2} - C_{s1}L_b\dot{w}_{w3} - K_{s1}L_b w_{w3}$$
$$- C_{s1}L_b\dot{w}_{w4} - K_{s1}L_b w_{w4} = 0 \tag{4.3}$$

where M_b is the mass of the bogie, J_b is the mass moment of inertia of the bogie, C_{s1} and C_{s2} are the primary and secondary suspension damping coefficients, K_{s1} and K_{s2} are the primary and secondary suspension spring constants, L_c is the distance between bogie centre lines, L_b is the distance between a bogie's wheelsets, g is the gravitational acceleration constant, and w and θ are the vertical displacements and angular displacements of the components with subscripts c, b, and w representing the carriage, bogie, and wheelset respectively.

Similarly, equations describing the motion for the remaining vehicle system components have been derived. For the carriage:

$$M_c\ddot{w}_c + 2C_{s2}\dot{w}_c + 2K_{s2}w_c - C_{s2}\dot{w}_{b1} - K_{s2}w_{b1}$$
$$- C_{s2}\dot{w}_{b2} - K_{s2}w_{b2} = M_c g \tag{4.4}$$

$$J_c\ddot{\theta}_c + 2C_{s2}L_c^2\dot{\theta}_c + 2K_{s2}L_c^2\theta_c + C_{s2}L_c\dot{w}_{b1} + K_{s2}L_c w_{b1}$$
$$- C_{s2}L_c\dot{w}_{b2} - K_{s2}L_c w_{b2} = 0 \tag{4.5}$$

For the trailing bogie:

$$M_{b1}\ddot{w}_{b1} + (C_{s2} + 2C_{s1})\dot{w}_{b1} + (K_{s2} + 2K_{s1})w_{b1} - C_{s2}(\dot{w}_c - L_c\dot{\theta}_c)$$
$$- K_{s2}(w_c - L_c\theta_c) - C_{s1}\dot{w}_{w1} - K_{s1}w_{w1} - C_{s1}\dot{w}_{w2} - K_{s1}w_{w2} = M_b g \tag{4.6}$$

$$J_{b1}\ddot{\theta}_{b1} + 2C_{s1}L_b^2\dot{\theta}_{b1} + 2K_{s1}L_b^2\theta_{b1} - C_{s1}L_b\dot{w}_{w3} - K_{s1}L_b w_{w3}$$
$$- C_{s1}L_b\dot{w}_{w4} - K_{s1}L_b w_{w4} = 0 \tag{4.7}$$

And for the wheelsets:

$$M_w \ddot{w}_{w1} + C_{s1}\dot{w}_{w1} + K_{s1}w_{w1} - C_{s1}(\dot{w}_{b1} - L_b\dot{\theta}_{b1})$$
$$- K_{s1}(w_{b1} - L_b\theta_{b1}) = M_w g - P_{wr1} \quad (4.8)$$

$$M_w \ddot{w}_{w2} + C_{s1}\dot{w}_{w2} + K_{s1}w_{w2} - C_{s1}(\dot{w}_{b1} + L_b\dot{\theta}_{b1})$$
$$- K_{s1}(w_{b1} + L_b\theta_{b1}) = M_w g - P_{wr2} \quad (4.9)$$

$$M_w \ddot{w}_{w3} + C_{s1}\dot{w}_{w3} + K_{s1}w_{w3} - C_{s1}(\dot{w}_{b2} - L_b\dot{\theta}_{b2})$$
$$- K_{s1}(w_{b2} - L_b\theta_{b2}) = M_w g - P_{wr3} \quad (4.10)$$

$$M_w \ddot{w}_{w4} + C_{s1}\dot{w}_{w4} + K_{s1}w_{w4} - C_{s1}(\dot{w}_{b2} + L_b\dot{\theta}_{b2})$$
$$- K_{s1}(w_{b2} + L_b\theta_{b2}) = M_w g - P_{wr4} \quad (4.11)$$

where M_c is the mass of the carriage, J_c is the mass moment of inertia of the carriage, M_w is the mass of the wheel, and P_{wr} is the contact force between the wheel and rail.

The above equations describe the complete vehicle system, consisting of ten degrees of freedom (DOF).

4.2.2   Rail track equations of motion

The track system consists of the rail modelled as a beam and supported by a spring-mass-damper system representing the sleepers and ballast. An FBD of the beam is provided in Figure 4.3.
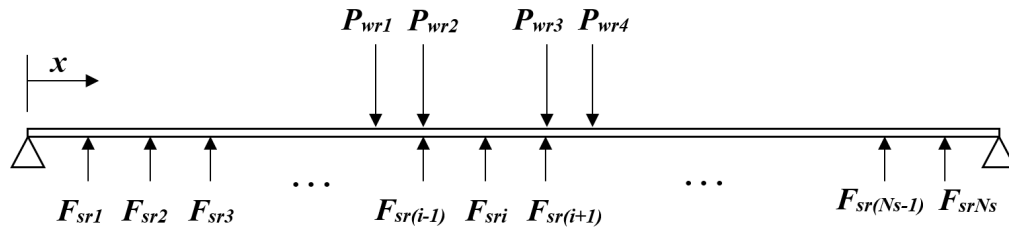
Figure 4.3: Free body diagram of Euler-Bernoulli beam rail

Equation 4.12 gives the equation for the beam according to the Euler-Bernoulli beam theorem:

$$EI\frac{\partial^4 w_r(x,t)}{\partial x^4} + m_r\frac{\partial^2 w_r(x,t)}{\partial t^2} = -\sum_{i=1}^{N_s} F_{sri}\delta(x-x_i) + \sum_{j=1}^{4} P_{wrj}\delta(x-x_i) \quad (4.12)$$

in which $\delta(x)$ is the Dirac-delta function, E is the rail modulus of elasticity, I is the rail cross section area moment of inertia, m_r is the rail mass per meter, w_r is the rail displacement, N_s is the number of sleepers, and F_{sr} is the force between the rail and sleeper.

Before this beam model definition could be incorporated into the model, it was necessary to transform the partial differential equation (PDE) into a set of ordinary differential equations (ODE). Having a set of ODE meant that the equations could be included within a matrix, along with the track equations of motion, which could then be explicitly solved at each time step. See Section 4.3 for further details on the solution method.

The principal of modal superposition was used to transform the PDE. Equation 4.13 approximates the deflection of the beam at a given location and time as the linear combination of a number of its mode shapes. The more mode shapes used in this calculation, the more accurate the deflection approximation becomes.

$$w_r = \sum_{n=1}^{N_m} \Phi_n(x)q_n(t) \quad (4.13)$$

where Φ_n and q_n are the nth mode shape function and mode time coefficient respectively, and N_m is the number of mode shapes.

Note that due to the pinned boundary conditions of the beam, the mode shapes take the form:

$$\Phi_n = \sin(\frac{n\pi x}{L_r}) \quad (4.14)$$

Substitution of Equation 4.13 into Equation 4.12 yields an ODE in terms of the variable q, given in Equation 4.15.

$$m_r\ddot{q}_n + EI\left(\frac{n\pi}{L_T}\right)^4 = -\sum_{i=1}^{N_s} F_{sri}\Phi_n(x_i) + \sum_{j=1}^{4} P_{wrj}\Phi_n(x_j) \quad (4.15)$$

where L_T is the total length of the rail, and $n = 1, 2, \ldots, N_m$.

The interaction forces for the sleepers can be expressed due to the deflection of the rail as:

$$F_{sri} = C_p\sum_{n=1}^{N_m} \Phi(x_i)\dot{q}_n + K_p\sum_{n=1}^{N_m} \Phi(x_i)q_n - C_p\dot{w}_{si} - K_p w_{si} \quad (4.16)$$

where C_p and K_p are the railpad damping and stiffness coefficients, and w_s is the sleeper displacement.

From Equation 4.16 the sleeper forces that are associated with the nth mode are:

$$F_{sri} = C_p \Phi(x_i)\dot{q}_n + K_p \Phi(x_i)q_n - C_p \dot{w}_{si} - K_p w_{si} \qquad (4.17)$$

Substitution of Equation 4.17 into Equation 4.15 yields the final equation of the beam, Equation 4.18, that is solved along with the equations of motion.

$$m_r \ddot{q}_n + EI\left(\frac{n\pi}{L_T}\right)^4 q_n + C_p \sum_{i=1}^{N_s} \Phi_n(x_i)\Phi_n(x_i)\dot{q}_n + K_p \sum_{i=1}^{N_s} \Phi_n(x_i)\Phi_n(x_i)q_n$$
$$- C_p \sum_{i=1}^{N_s} \Phi_n(x_i)\dot{w}_{si} - K_p \sum_{i=1}^{N_s} \Phi_n(x_i)w_{si} = \sum_{j=1}^{4} P_{wrj}\Phi_n(x_j) \quad (4.18)$$

The remaining equations used to describe the track consist of the equations of motion for the sleeper and ballast. These are derived in the same way as the vehicle equations and are given in Equations 4.19 and 4.20 respectively. Note that the continuity of the ballast in the longitudinal direction is modelled through the use of massless viscoelastic elements connecting the consecutive ballast masses.

$$M_s \ddot{w}_{si} + (C_p + C_{bl})\dot{w}_{si} + (K_p + K_{bl})w_{si}$$
$$- C_{bl}\dot{w}_{bli} - K_{bl}w_{bli} - C_p \sum_{n=1}^{N_m} \Phi_n(x_i)\dot{q}_n - K_p \sum_{n=1}^{N_m} \Phi_n(x_i)q_n = 0 \quad (4.19)$$

$$M_{bl}\ddot{w}_{bli} + (C_{bl} + C_{sg} + 2C'_{bl})\dot{w}_{bli} + (K_{bl} + K_{sg} + 2K'_{bl})w_{bli}$$
$$- C_{bl}\dot{w}_{si} - K_{bl}w_{si} - C'_{bl}(\dot{w}_{bl(i-1)} - \dot{w}_{bl(i+1)}) - K'_{bl}(w_{bl(i-1)} - w_{bl(i+1)}) \quad (4.20)$$

where M_s is the sleeper mass, M_{bl} is the ballast mass, C_{bl} and K_{bl} are the ballast damping and stiffness coefficients, C_{sg} and K_{sg} are the subgrade damping and stiffness coefficients, w_{bl} is the ballast vertical displacement, and C'_{bl} and K'_{bl} are the damping and stiffness coefficients of the viscoeslastic elements connecting each ballast block to its neighbouring ballast blocks.

For each mode shape used to describe the beam, the system has a DOF in q. For each discrete support, the system has another DOF each for the sleeper and ballast. As an example, a track described by 50 mode shapes and 50 sleepers would result in a 150 DOF system. Zhai and Sun (1994) shows that for acceptable convergence in rail deflection, more than 60 mode shapes are required to describe the beam.

The ballast in the track system is modelled using the ballast pyramid model developed by Ahlbeck *et al.* (1975). This model is depicted in Figure 4.4 and provides an effective method to model the continuous ballast as a lumped mass system. H_{bl} represents the effective height of the ballast, L_l represents the effective length of the support area, and B_l represents the effective width of the support area.
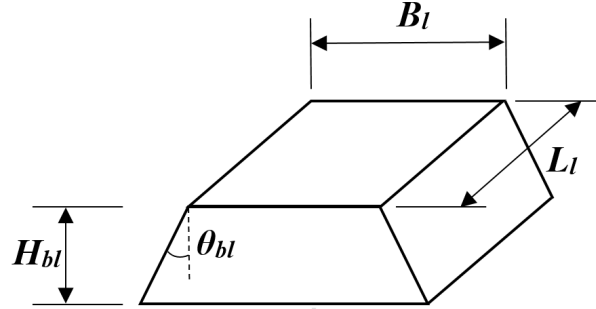
Figure 4.4: Ballast pyramid model

The expressions for the ballast mass and stiffness derived from this model are given in Equations 4.21 and 4.22 respectively. Ahlbeck *et al.* (1975) recommends a value of 20° for the ballast internal friction angle θ_{bl}.

$$M_{bl} = \rho_{bl} \left[L_l B_l + H_{bl} \tan \theta_{bl}(L_l + B_l) + \frac{4}{3} H_{bl}^2 \tan^2 \theta_{bl} \right] \quad (4.21)$$

$$K_{bl} = \frac{2 \tan \theta_{bl}(L_l - B_l) E_{bl}}{\ln \left(\frac{L_l}{B_l} \frac{B_l + 2 \tan \theta_{bl} H_{bl}}{L_l + 2 \tan \theta_{bl} H_{bl}} \right)} \quad (4.22)$$

where ρ_{bl} is the ballast density and E_{bl} is the ballast modulus of elasticity

Equation 4.23 for the subgrade stiffness was adapted from Sun and Dhanasekar (2002), in which the stiffness is the product of the elastic modulus of the subgrade and the contact area between the ballast and subgrade.

$$K_{sg} = E_{sg}(2 \tan \theta_{bl} H_{bl} + L_l)(2 \tan \theta_{bl} H_{bl} + B_l) \quad (4.23)$$

where E_{sg} is the elastic modulus of the subgrade.

Sun and Dhanasekar (2002) recommends that the damping coefficients for the ballast and subgrade be set to 40% of their critical values, which is a realistic damping ratio for earth structures. They also show that the values obtained using this damping ratio are within the range proposed by Grassie *et al.* (1982).

The coefficients of the viscoelastic elements used to model ballast continuity are determined by Sun and Dhanasekar (2002) as the ballast stiffness or

damping multiplied by a factor of 0.3. They show that this factor in insensitive to the dynamic responses at the rail vehicle and track interface.

4.2.3   Interface between vehicle and track

The rail vehicle equations of motion (Equations 4.2 to 4.11) and rail track equations (Equations 4.18 to 4.20) are combined to give the matrix Equations 4.24 and 4.25. These two matrix equations represent the dynamics of the vehicle and track respectively.

$$[M_V]\{\ddot{w}_V\} + [C_V]\{\dot{w}_V\} + [K_V]\{w_V\} = \{F_V\} \tag{4.24}$$

$$[M_T]\{\ddot{w}_T\} + [C_T]\{\dot{w}_T\} + [K_T]\{w_T\} = \{F_T\} \tag{4.25}$$

where

$$\{w_V\} = \{w_c \ \theta_c \ w_{b1} \ \theta_{b1} \ w_{b2} \ \theta_{b2} \ w_{w1} \ w_{w2} \ w_{w3} \ w_{w4}\}^T$$

$$\{w_T\} = \{q_1 \ q_2 \ \cdots \ q_{N_m} \ w_{s1} \ w_{s2} \ \cdots \ w_{sN_s} \ w_{bl1} \ w_{bl2} \ \cdots \ w_{blN_s}\}^T$$

The contact force between the wheel and rail is modelled using non-linear Hertz contact theory, as shown in Equation 4.26.

$$P_{wrj} = \begin{cases} C_H(w_{wj} - w_r(x_{wj}) - w_{irr})^{3/2} & \text{if } (w_{wj} - w_r(x_{wj}) - w_{irr}) > 0 \\ 0 & \text{if } (w_{wj} - w_r(x_{wj}) - w_{irr}) < 0 \end{cases} \tag{4.26}$$

where w_{wj} is the displacement of the jth wheel, $w_r(x_{wj})$ is the rail displacement at the jth wheel, and w_{irr} represents a wheel or track irregularity such as those described in Table 4.1.

The Hertz contact coefficient, C_H, can be determined through use of Equation 4.27 (Johnson, 1985).

$$C_H = \frac{4G\sqrt{R_w\left(\frac{r_w r_p}{r_w - R_w}\right)}}{3(1 - \nu)} \tag{4.27}$$

where G is the shear modulus, ν is the Poisson's ratio, R_w is the wheel rolling radius, r_w is the wheel profile radius, and r_p is the rail profile radius.

4.3   Solution of the dynamic model

The model is solved by applying the Newmark-β numerical integration scheme to Equations 4.24 and 4.25. For more information on this numerical integration scheme please refer to Appendix B.

Irregularities are modelled on the rail or wheel during the simulation in order to obtain the rail vehicle's operational response. These irregularities can be used to model real world operational flaws such as wheel flats or corrugations on the rail. Some examples of irregularities are given in Table 4.1 (Sun and Dhanasekar, 2002).
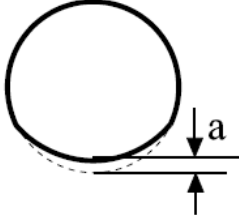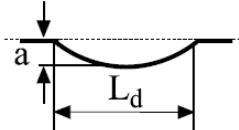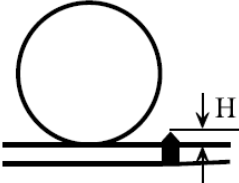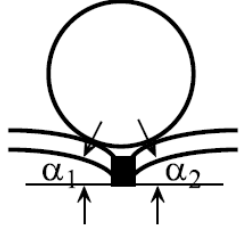
Type and geometry	Mathematical expression
Harmonic excitation	
Wheel flat	$w_{irr} = \frac{a}{2}\left(1 - \cos\left(\frac{2\pi V t}{L_d}\right)\right)$
Indentation on rail surface	$w_{irr} = \frac{a}{2}\left(1 - \cos\left(\frac{2\pi V t}{L_d}\right)\right)$
Impulse excitation	
Raise on weld joint	$V_{impulse} = V\left(\sqrt{\frac{2H}{R_w}}\right)$
Dipped joint	$V_{impulse} = V(\alpha_1 + \alpha_2)$

Table 4.1: Examples of track/wheel irregularities Sun and Dhanasekar (2002)

As the rail vehicle is simulated moving through these irregularities, the vertical interactions throughout the vehicle or track can be extracted. In this case, the interactions at the primary and secondary suspensions are the main concern.

4.4   Validation of the dynamic model

The model has been validated against numerical models published in literature, the first by Zhai *et al.* (2001). In their study, they present the experimental and numerical wheel-rail contact force determined for a freight car wheel. The wheel in question included a rounded wheel flat, the expression for which is given in Table 4.1. The experimental results were obtained by the Luoyang Rolling Stock Maintenance Department in China. The vehicle was travelling at 27 km/h during measurement. The results can be seen in Figure 4.5.
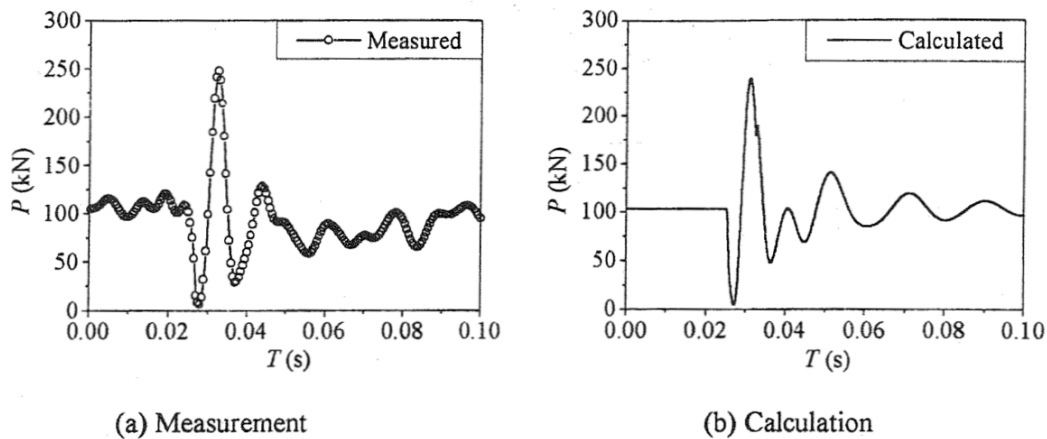
Figure 4.5: Wheel-rail contact force response due to wheel flat reported by Zhai *et al.* (2001)

Figure 4.6 shows the results obtained from the model developed here, using the parameters reported by Zhai *et al.* (2001). The results of these models show a decrease in contact force as the irregularity is encountered, due to the separation of the wheel and rail. Following the decrease is a sharp increase in contact force due to impact between the wheel and rail. This impact is referred to as the P_1 force (Zhai *et al.*, 2001).

It can be seen that the two models agree with each other relatively well, especially in the prediction of the P_1 force. The differences in the model are attributed to the fact that not all the necessary parameters were provided by Zhai *et al.* (2001). The missing parameters include the Hertz contact coefficient and the primary suspension characteristics. The Hertz contact coefficient was assumed based on those given by Sun and Dhanasekar (2002). The primary

suspension characteristics were assumed to be rigid for this simulation. This
is due to the fact that freight trains do not make use of primary suspensions,
and the wheelsets are directly connected to the bogie.
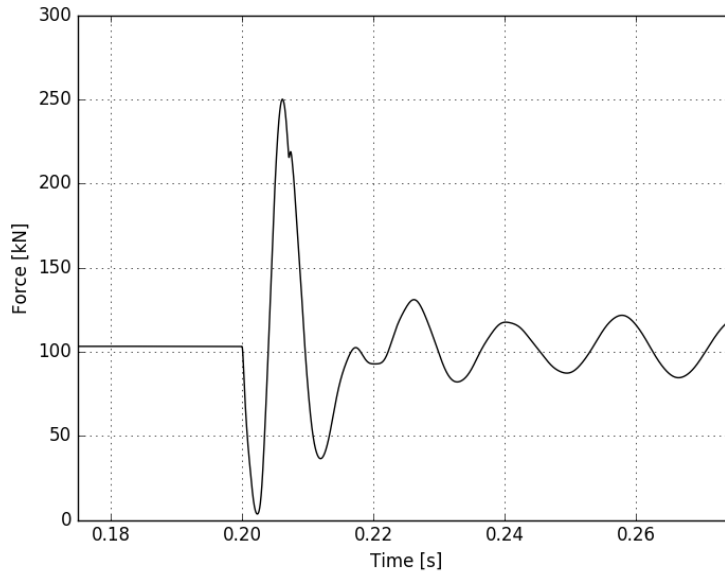
Figure 4.6: Wheel-rail contact force response due to wheel flat for model developed
here

The second case from literature is the application of the model developed
by Sun and Dhanasekar (2002) to the experimental results provided by New-
ton and Clark (1979). The data published by Newton and Clark (1979) was
obtained through experimental measurements of the wheel-rail contact force
as the vehicle travelled through a long indentation on the rail. The vehicle
was travelling at 117 km/h during measurement. As Newton and Clark (1979)
provided very few vehicle and track parameters, Sun and Dhanasekar (2002)
assumed parameters based a well known system used in Australia. The exper-
imental and numerical results can be seen in Figure 4.7.

Sun and Dhanasekar (2002) attribute the difference between the experi-
mental and numerical results in Figure 4.7 to the damping coefficients of the
pad and sleeper in the model. They show that the contact force is sensitive to
these parameters, and as they use assumed values there results differ.

The results obtained using the developed model with the parameters pro-
vided by Sun and Dhanasekar (2002) are presented in Figure 4.8.

It can be seen that the results of the developed model differ slightly from the
results provided by Sun and Dhanasekar (2002). The difference is attributed
to the use of the Euler-Bernoulli beam formulation used in the modelling of the
rail. Sun and Dhanasekar (2002) made use of the Timoshenko beam theory
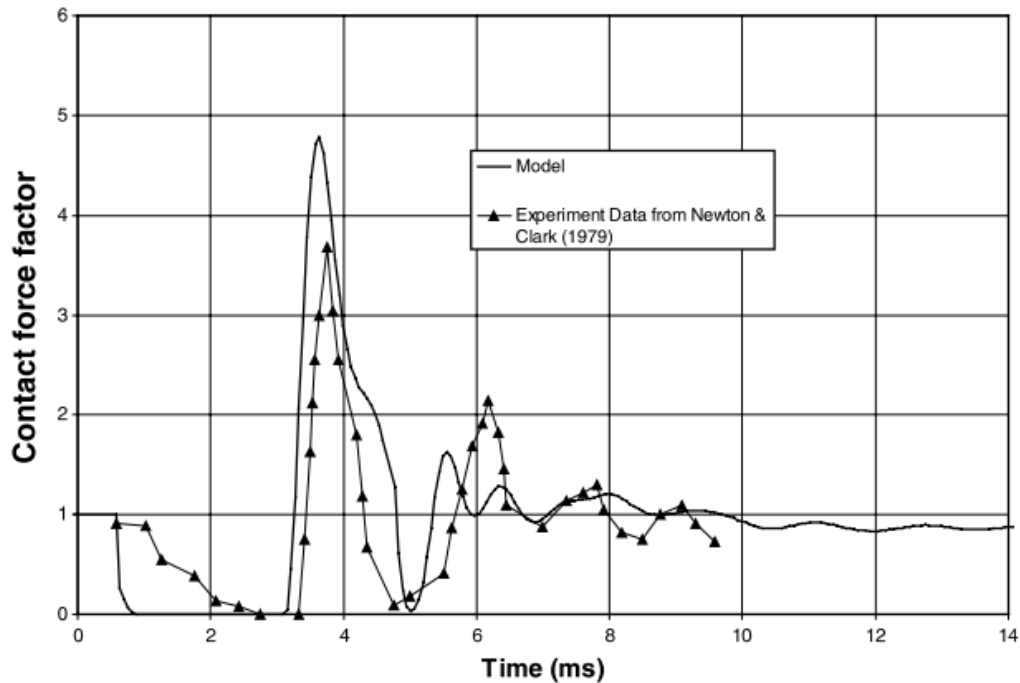
Figure 4.7: Wheel-rail contact force factor due to rail indentation from Sun and Dhanasekar (2002)

to model their rail, which provides a better response at higher frequencies. Though the developed model predicts a P_1 force that is close to that of Sun and Dhanasekar (2002), it is shown that this model is more accurate for lower frequency responses. Both models over predict the experimental contact force due to the assumed parameters.

This validated model can be used to extract the interaction forces at the primary and secondary suspension. The extracted forces can be multiplied with the stress distribution of the bogie due to unit loads and superimposed to obtain stress histories. The finite element model used to obtain the bogie stress distribution is discussed in the following chapter.
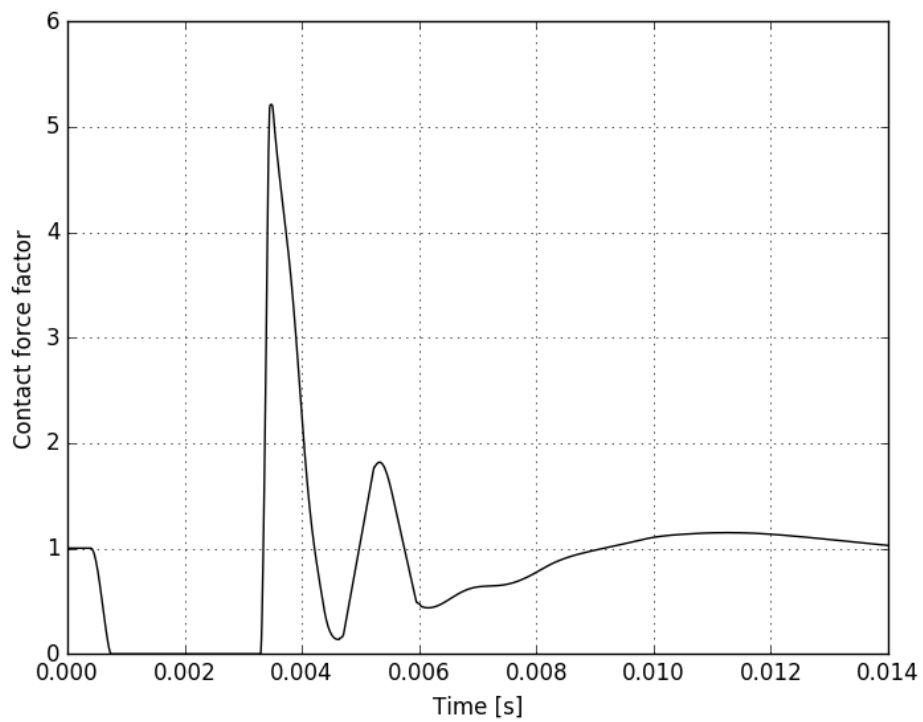
Figure 4.8: Wheel-rail contact force factor due to rail indentation for developed model using parameters from Sun and Dhanasekar (2002)

Chapter 5

Finite Element Modelling

This chapter presents the creation of the FE model of the class 5M bogie frame. This FE model is used to determine the stress distribution within the bogie due to loads experienced at the primary and secondary suspension attachment areas.

5.1 Three dimensional model of the bogie assembly

A three dimensional CAD model of the full bogie assembly has been provided by the PRASA Engineering Research Chair and is shown in Figure 5.1. This CAD model contains the bogie frame and the various components it houses, such as the primary and secondary suspensions, the traction motors, the wheelsets, and the brake rigging. Data from a three dimensional scan of an existing bogie frame was used to produce the provided drawing of the bogie frame.

The component of interest in the study is the bogie frame, pictured in Figure 5.2. It is this component that the fatigue study is focused on.

5.2 Finite element model of the bogie frame

In order to aid possible future research in this area, it was decided not to simplify the bogie frame model and instead create a complex FE model. Thus the entire frame, including elements such as the attachments for the brake rigging, was modelled. It is also worth noting that the bogie frame is a cast structure, meaning that there is no need to take account of welding in the FE analysis. Welding can often cause issues in FE analysis that must be taken into account such as residual stresses or localised material variation.

The FE model was constructed using MSC Apex. This software was chosen because of the powerful tools available for geometry manipulation and meshing.
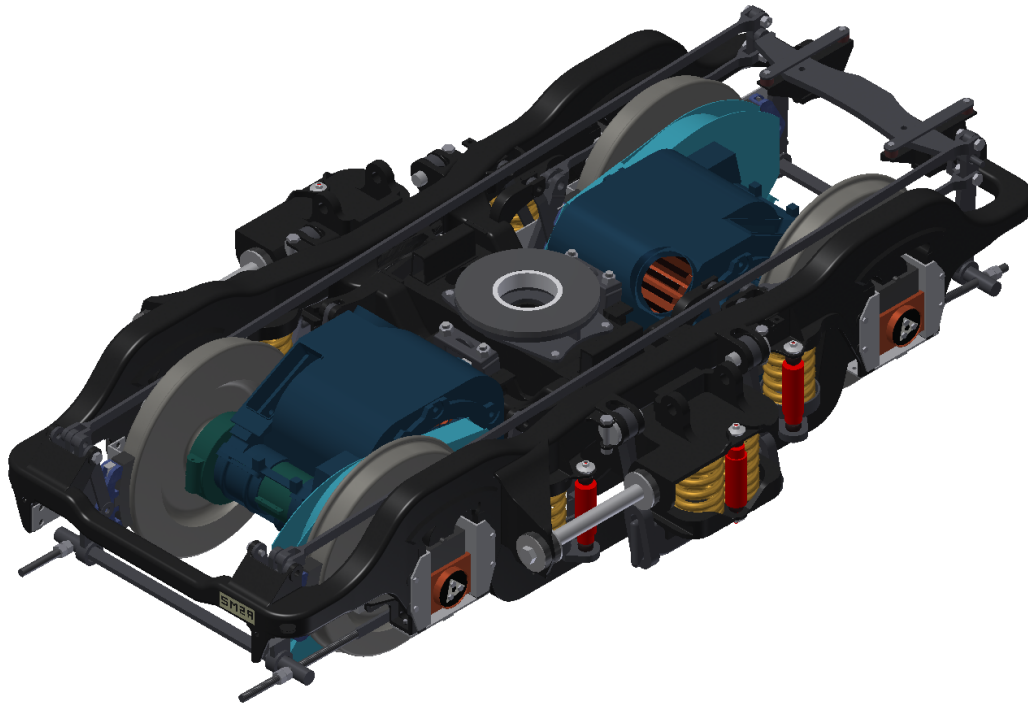
Figure 5.1: Three dimensional model of 5M bogie assembly

Figure 5.2: Three dimensional model of 5M bogie frame

Due to the thin-walled nature of the bogie frame design, the FE model was constructed using the midsurfaces of the bogie frame CAD model. Though this is a simplification that may not be valid throughout the bogie structure, it was necessary to reduce the number of elements that were modelled.

These surfaces were then meshed using linear shell elements. The FE model also made use of symmetry so only half of the frame was modelled. This is acceptable in this case as the loads from the dynamic model were also assumed to be symmetric. Had the dynamic model been constructed to take into account different irregularities on either rail, the loads on either side of the bogie would differ and a full model would be required.

The intent for the FE model is to provide a separate stress field for each load at the suspension attachment areas. These fields can then be scaled by a factor, such as the dynamic loads obtained using the model in Chapter 4, at each time step and superimposed to determine the entire stress distribution in the bogie. In this way, a resource intensive transient simulation is not necessary and is replaced with a single static simulation utilizing several load cases.

5.2.1 Boundary conditions

The boundary conditions consist of symmetry boundary conditions and the implementation of inertia relief to remove rigid body modes. Inertia relief was used as it was a close representation of the actual operating conditions. This technique allows for the analysis of unconstrained structures by calculating the sum of the forces and moments applied to the structure, and applying an equivalent inertial load to force a state of equilibrium. This is equivalent to the sum of the loads applied to structure being equal to the product of the structure's mass and acceleration. The inertia relief method determines and applies the acceleration necessary for a state of dynamic equilibrium. Introducing further boundary conditions, other than those required for symmetry, would artificially stiffen the bogie frame.

Rangwala (2006) states that using inertia relief along with symmetry boundary conditions is acceptable on condition that the reaction forces are zero at the symmetry constraints, so that the model is not over constrained. To confirm this statement, a small pilot study was conducted using a simple beam element model of a bogie frame and simulated using the MSC Patran/Nastran environment. Figure 5.3 shows the model used for this pilot study and Table 5.1 presents the results.

The model was solved using inertia relief, first on a full model and then a half model. It was seen that both models returned the same stress results. The displacement results of the inertia relief simulations give relative displacements and each model had different reference nodes. However it was found that the stress was the same irrespective of the reference node selected.

At any given point in the load history of the bogie frame, it would be subject to unbalanced loads causing a non-zero acceleration. The models in the pilot

(a) Full model

(b) Symmetric model
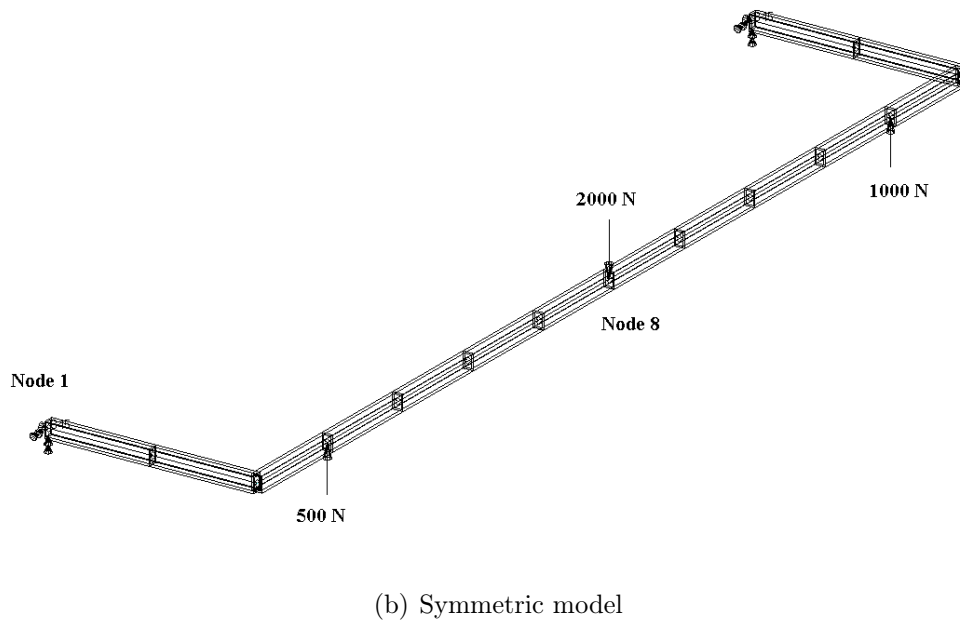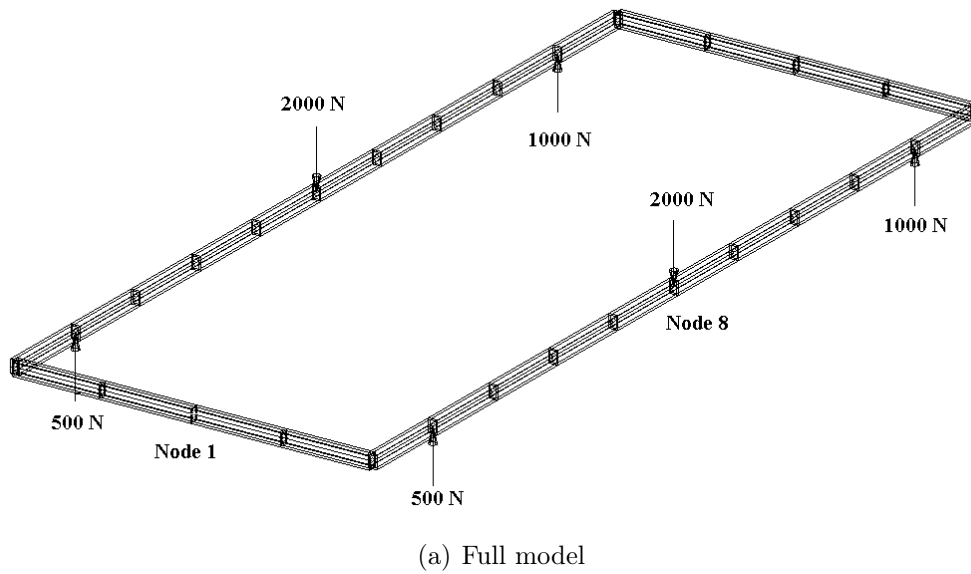
Figure 5.3: Pilot model used to investigate symmetry and inertia relief

study were also simulated using unbalanced loads. This verifies that the inertia relief method is applicable not only to static simulations of unconstrained structures, but also to structures that experience non-zero accelerations.

Table 5.1: Results of pilot study to investigate symmetry and inertia relief

Model	Stress at node 8
Full model	1.58 GPa
Symmetric model with inertia reference node 1	1.58 GPa
Symmetric model with inertia reference node 8	1.58 GPa

5.2.2   Superposition

It was also necessary to investigate the effect of inertia relief on the superposition of the FE model. The principle of superposition states that a structure subjected to multiple loads can be analysed by taking the contribution of each load and summing them to determine the combined effects of the loads.

To this end, the pilot study of Section 5.2.1 was extended and the symmetric model simulated under each of its applied loads separately. The results in Table 5.2 show that using superposition with inertia relief still achieves the correct result.

Table 5.2: Results of pilot study to investigate superposition and inertia relief

Model	Stress at node 8
Symmetric model with 500 N load	0.08 GPa
Symmetric model with 2 kN load	1.34 GPa
Symmetric model with 1 kN load	0.16 GPa
Symmetric model with all loads	1.58 GPa

5.2.3   Convergence of the finite element model

Once it was confirmed that the assumptions made with regards to inertia relief and its influence on symmetry and superposition were correct, the shell model's convergence was investigated. This was done by applying 1 kN loads at the primary and secondary suspension attachment points and monitoring the maximum stress hotspots. This load case is representative of the static load that will be experienced by the bogie. The plot in Figure 5.4 shows the stress convergence at said hotspot. These results are also tabulated in Table 5.3.

Table 5.3: Convergence of bogie finite element model using shell elements

Number of elements	Hotspot stress
19 039	1.48 MPa
67 224	2.00 MPa
255 986	2.28 MPa
1 544 542	2.15 MPa
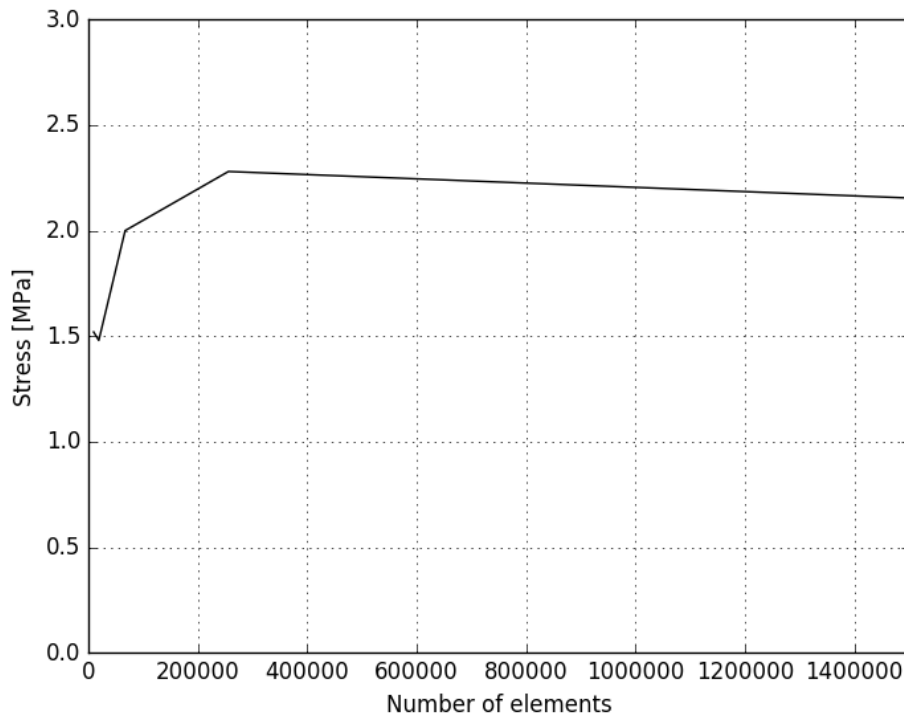
Figure 5.4: Convergence of bogie finite element model using shell elements

It can been seen that the convergence of the model is irregular. Upon closer inspection of the elements at the hotspot location, it was noted that stress discontinuities are present. This is due to sharp re-entrant corners that are present in the area. The stress discontinuity is displayed in Figure 5.5. Here it can be seen that a single element displays a high stress while the neighbouring elements experience much lower stresses.

The presence of the discontinuity results in inaccurate fatigue life calculations for the nearby elements. Due to the high risk of this area for fatigue failure, it was decided to incorporate a solid mesh to obtain more accurate stress results for fatigue analysis. Figure 5.6 shows the stress results at the hotspot using solid elements.

The inclusion of the solid mesh creates further stress discontinuities at the interface between shell and solid elements, however as these areas are known to not be of concern with a full shell mesh or a full solid mesh under the same load case, these discontinuities can be ignored. Furthermore, the solid mesh removes the possibility of errors due to the thin-walled assumption in the areas of interest.

With the solid elements incorporated, the convergence is reinvestigated. Figure 5.7 shows the convergence of the solid elements and the results are also tabulated in Table 5.4.
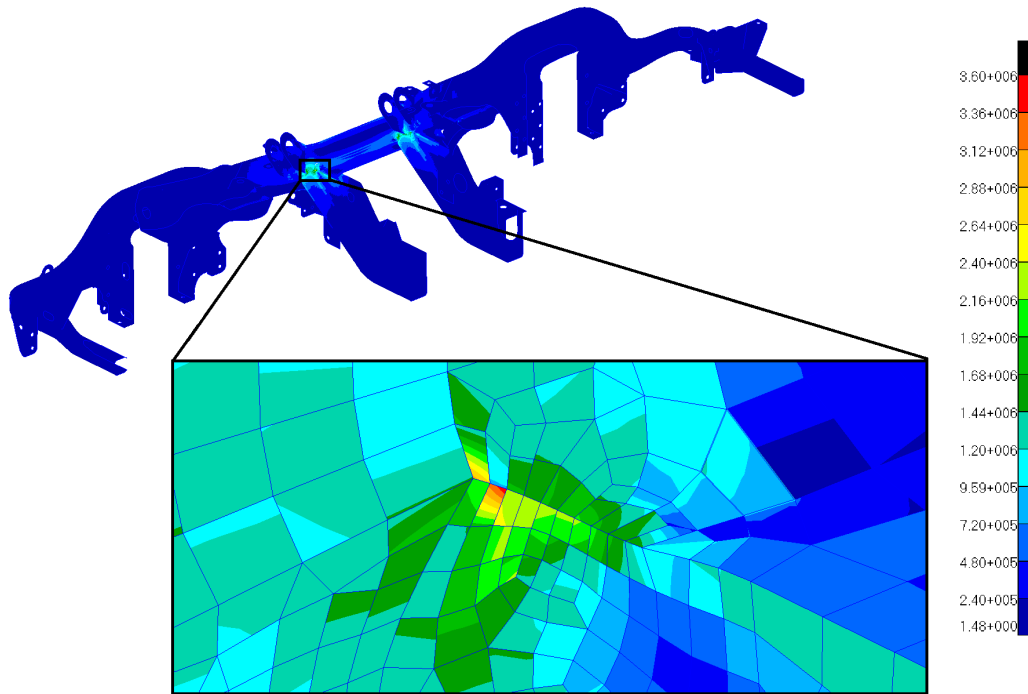
Figure 5.5: Stress distribution at hotspot using shell elements, showing stress discontinuities

Table 5.4: Convergence of bogie finite element model using solid elements

Number of elements	Hotspot stress
57 859	1.97 MPa
94 391	2.66 MPa
293 176	3.05 MPa
1 096 937	3.38 MPa
3 839 280	3.53 MPa

5.2.4   Details of final finite element model

The final shell FE model is presented in Figure 5.8 with a summary provided in Table 5.5. The material properties used for this model are those typical of steel, Table 5.6. Though these are not the correct properties for the bogie structure, they are sufficiently representative for the development of the model.

Table 5.5: Summary of finite element model of bogie frame

Number of elements	172 031
tet10	102 400
quad4	66 969
tria3	2 662
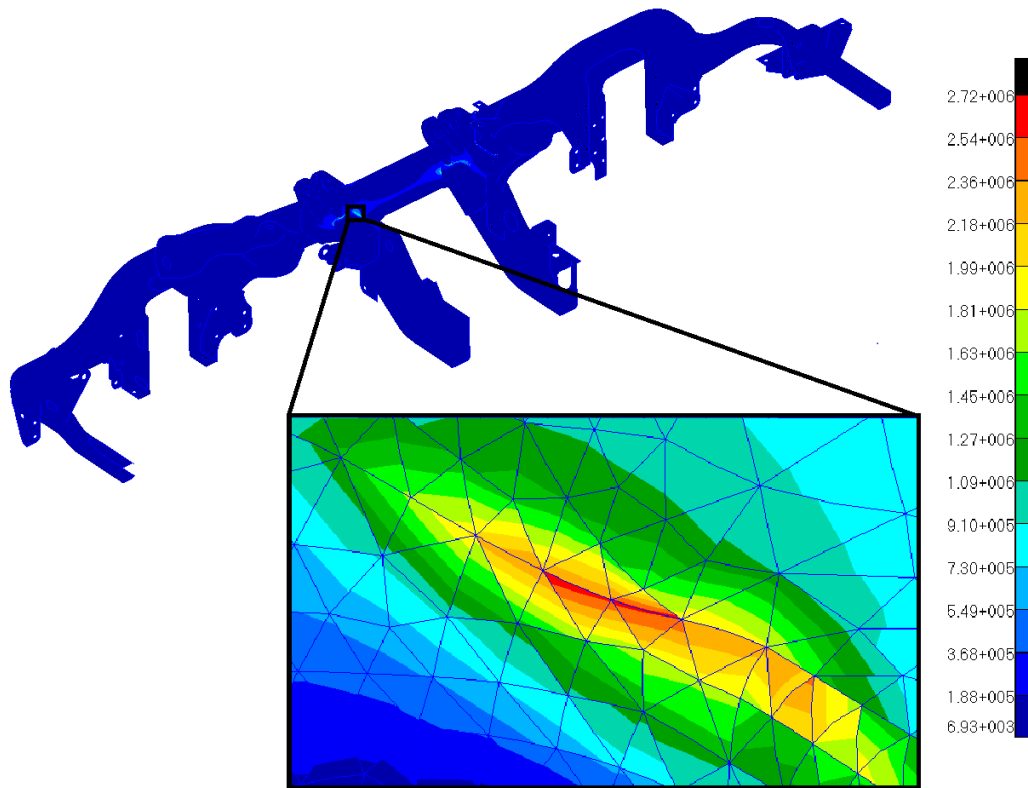
Figure 5.6: Stress distribution at hotspot using solid elements

Table 5.6: Typical material properties for steel

Property	Value
Modulus of elasticity	200 GPa
Poisson's ratio	0.3
Density	7850 kg/m^3
Yield strength	260 MPa
Ultimate tensile strength	490 MPa

The mesh for the final FE model of the bogie frame was obtained by applying a surface mesh to the midsurfaces of the bogie frame. The thickness and offset properties of each element were derived using the solid CAD model of the bogie frame. Solid elements were introduced to reduce stress discontinuities in areas of high risk fatigue failure. Stress hotspots were identified during the convergence study and the mesh has been refined in these areas only. This allows the use of relatively few elements overall while still having a significant number of elements in the regions of interest.

The stress distribution in the bogie frame, due to unit loads applied at the suspension attachments, is then determined. Figure 5.9 shows where these loads were applied. Note that the secondary suspension load has been split
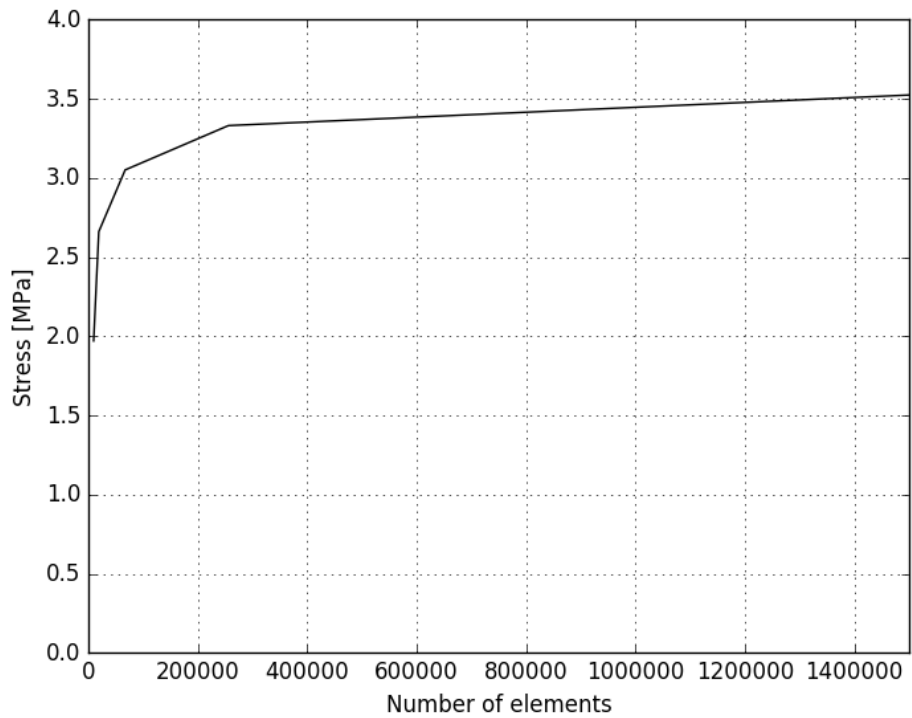
Figure 5.7: Convergence of bogie finite element model using solid elements
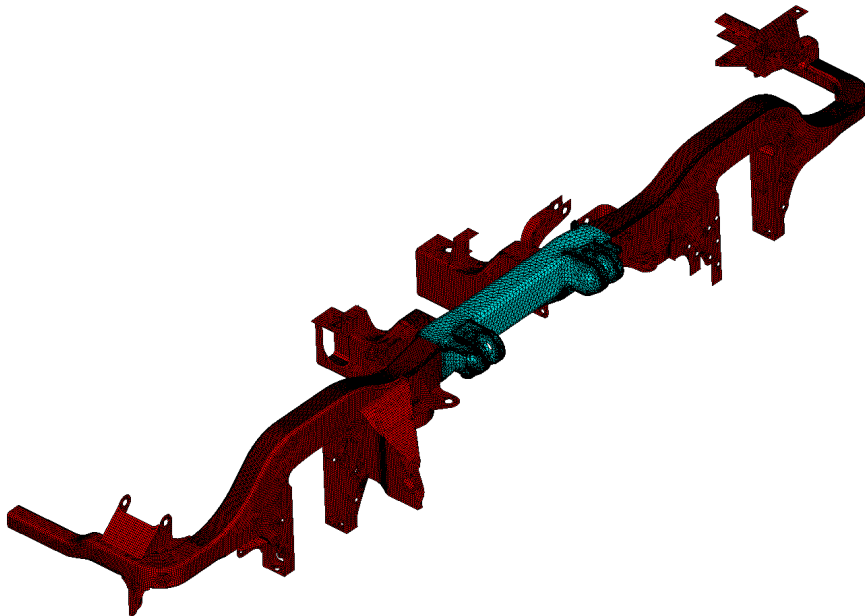
Figure 5.8: Finite element model of bogie frame: Shell elements are represented in red, while solid elements are cyan

the secondary suspension is attached to the bogie at two points. The loads were applied to the bogie as point loads distributed across the suspension attachment areas via use of RBE3 elements. As the areas of interest with regards to stress are relatively far from the load points, any localised effects introduced at the load points do not affect the stress results at the areas of interest. A static simulation is performed using the final mesh of the bogie frame. The simulation consists of three separate load cases, each having a single unit load of 1 kN applied at one of the two primary suspensions or the secondary suspension, with the 1 kN load split at two attachment points in the case of the secondary suspension.
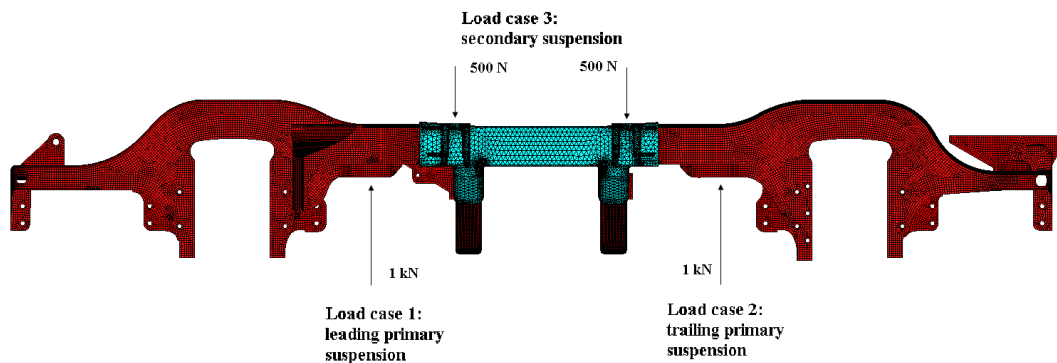
Figure 5.9: Load cases applied to bogie frame: Shell elements are represented in red, while solid elements are cyan

A load of 1 kN rather than 1 N was used to prevent large errors during superposition. When the simulation is performed, an area of zero stress will in fact have a stress value due to numerical noise. This numerical noise will be multiplied and superimposed leading to errors. By using a 1 kN load, the noise is at least a factor of 1 000 smaller than the stresses of interest.

The three stress distributions, one for each suspension, can then be multiplied with the dynamic load histories determined using the model in Chapter 4. This is done assuming that the bogie frame structure remains within the linear range.

For the bogie frame structure to remain within the linear range, the following conditions must hold:

- The material must be linear. This is assumed in the defenition of the material properties.

- Material deformations are small and the material does not yield. This is a fair assumption as railway bogie frames are designed for high-cycle

to infinite fatigue lives, and will most likely not be subjected to loads causing the structure to yield.

The stress histories can then be superimposed to provide the full stress history of the bogie frame. Finally, this stress history can be analysed using the fatigue script developed in the following chapter to estimate the fatigue life of the bogie frame.

Chapter 6

Fatigue Simulation

This chapter focuses on the fatigue simulation script that has been developed, using Python v2.7, for use in this study. The script is capable of receiving stress histories from a source and returning cumulative damage parameters and cycles to failure for those histories.

6.1 Stress-life method

The developed script makes use of the S-N approach, as opposed to the ϵ-N or fracture mechanics approaches. The script can however be expanded to include these approaches if the need arises in future work.

The S-N approach was selected because of the expectation that the bogie has a high cycle fatigue life. Typically, the ϵ-N approach is preferred for low cycle fatigue applications. For high cycle fatigue, where elastic strain dominates, the ϵ-N and S-N based approaches are equivalent (Dowling, 2007).

In order to predict the fatigue life using the S-N approach, an S-N curve is necessary. This curve predicts the number of cycles to failure at a specified stress amplitude. The S-N curve for the assumed material properties, Table 5.6, is estimated based on a process outlined in Budynas and Nisbett (2011). For a more detailed view on how S-N curves are estimated, please see Appendix C. The estimated S-N curve for these properties using completely reversed loads (mean stress is equal to zero) is shown in Figure 6.1. Note that the S-N curve must be obtained based on completely reversed loads. This is because the stress levels compared to the S-N curve are corrected based on their mean stress values. The correction is done in order to obtain an equivalent stress level at zero mean stress which can then be compared to the S-N curve. Further details on the mean stress correction are provided in Section 6.3.

38
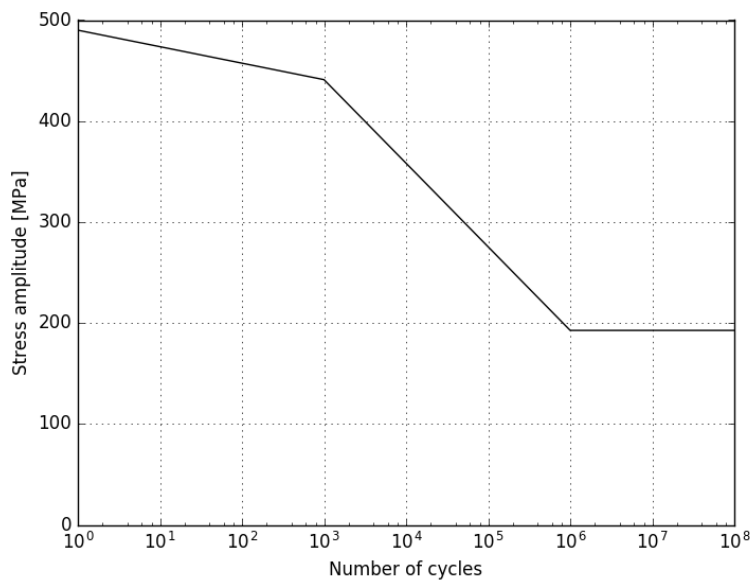
Figure 6.1: Estimated S-N curve using typical steel properties

6.2 Stress cycle counting

As the stress history used to predict fatigue life often contains cycles at various amplitudes, it is necessary to use a cycle counting method to determine how many cycles are experienced at each stress amplitude.

The cycle counting method chosen for this study is rainflow counting. The reasons for this are:

- Fuchs and Stephens (1980) state that good counting methods count every portion of each overall range once and only once. They further state that there are three well documented methods that achieve this: range-pair, rainflow, and racetrack counting.

- Dowling (1971) shows that methods other than range-pair and rainflow counting can result in inconsistencies and significant differences between actual and predicted fatigue lives.

- Both Dowling (2007) and Suresh (1991) state that the most widely used cycle counting method is rainflow counting.

The rainflow cycle counting method has been implemented using the algorithm provided by the ASTM E1049-85 standard (ASTM E1049-85, 2011). The counting method works as follows: let X denote the range under consideration, Y the previous adjacent range, and S the starting point in the cycle history. The following steps are then performed as outlined in ASTM E1049-85 (2011):

1. Read following peak or valley. If there is no remaining data then go to step 6

2. If there are less then three peaks/valleys in memory then go to step 1. Form ranges X and Y using the three most recent peaks/valleys that have not yet been discarded.

3. Compare the absolute values of X and Y.

   if $X < Y$ then go to step 1

   if $X \geq Y$ then go to step 4

4. If range Y contains starting point S then go to step 5, otherwise: count range Y as one cycle, discard the valley and peak of Y, and go to step 2.

5. Count range Y as one half cycle and discard the first point (peak or valley) in Y. Move the starting point S to the second point in range Y and then go to step 2.

6. Count each range not previously counted as a half cycle.

An example of this counting method taken from the standard is shown in Figure 6.2. The cycle history is counted as follows:

1. $S = A$; $Y = |A - B|$; $X = |B - C|$; $X > Y$; Y contains S so count A-B as a half cycle and discard point A; $S = B$. Figure 6.2b.

2. $Y = |B - C|$; $X = |C - D|$; $X > Y$; Y contains S so count B-C as a half cycle and discard point B; $S = C$. Figure 6.2c.

3. $Y = |C - D|$; $X = |D - E|$; $X < Y$.

4. $Y = |D - E|$; $X = |E - F|$; $X < Y$.

5. $Y = |E - F|$; $X = |F - G|$; $X > Y$; Y does not contains S so count E-F as one cycle and discard points E and F. Figure 6.2d. Note: a cycle is formed by pairing range E-F and a portion of range F-G.

6. $Y = |C - D|$; $X = |D - G|$; $X > Y$; Y contains S so count C-D as a half cycle and discard point C; $S = D$. Figure 6.2e.

7. $Y = |D - G|$; $X = |G - H|$; $X < Y$.

8. $Y = |G - H|$; $X = |H - I|$; $X < Y$. End of data.

9. Count ranges D-G, G-H, and H-I as half cycles. Figure 6.2f.

10. End counting.
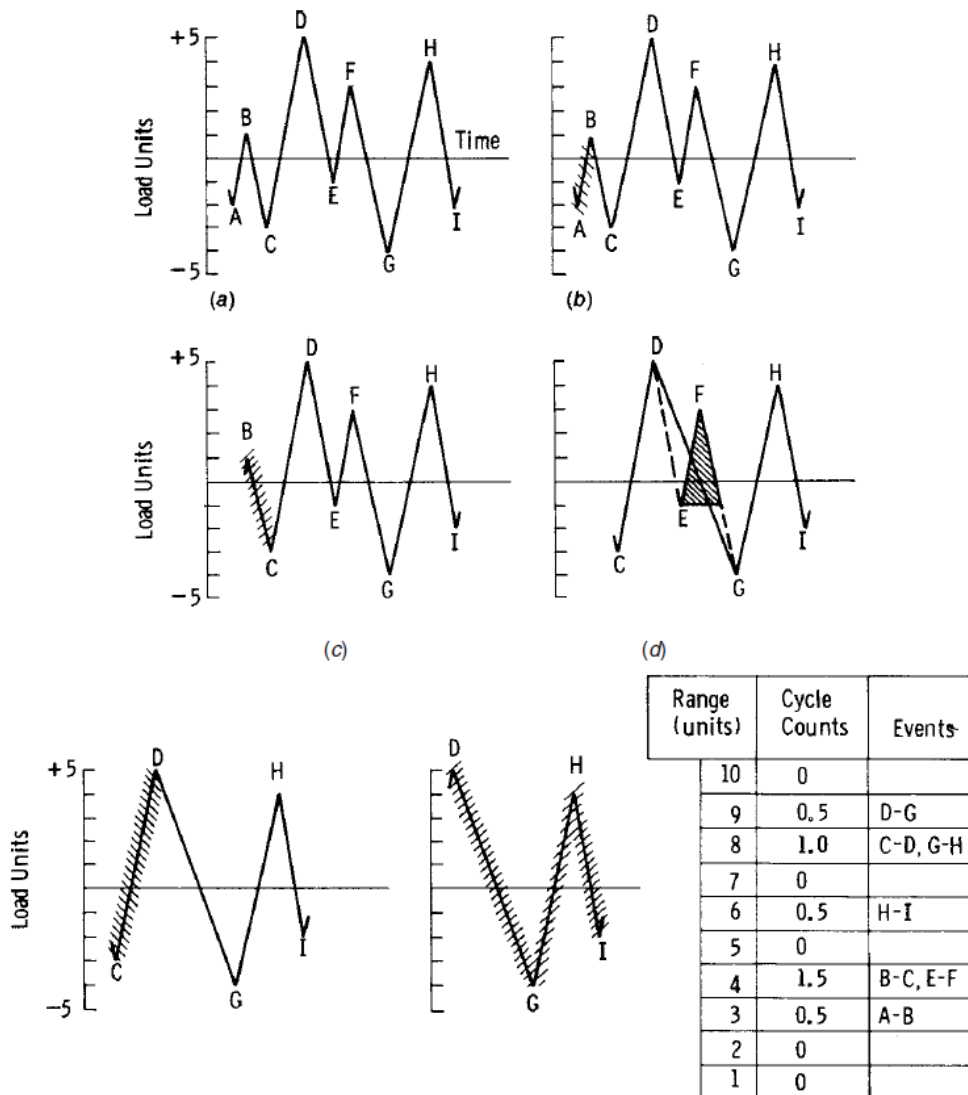
Figure 6.2: Example of rainflow cycle counting (ASTM E1049-85, 2011)

As each range is counted, as either a full or half cycle, the stress amplitude (σ_a) and mean stress (σ_m) for that range is also determined using Equations 6.1 and 6.2 respectively. The number of cycles to failure for a given stress amplitude can then be determined by comparing it to the S-N curve after it is been corrected for its mean stress value.

$$\sigma_m = \frac{\sigma_{max} + \sigma_{min}}{2} \tag{6.1}$$

$$\sigma_a = \left| \frac{\sigma_{max} - \sigma_{min}}{2} \right| \tag{6.2}$$

where σ_{max} and σ_{min} are the maximum and minimum values in the range respectively.

6.3 Mean stress correction

Before the equivalent stresses can be compared to the S-N curve, they must be corrected for mean stress. The effect of mean stress has been included as tensile mean stress will reduce fatigue life, as shown by Frost *et al.* (1974). They also show that should the mean stress be compressive the fatigue life may be extended. They suggest, however, that a compressive mean stress be treated as a zero mean stress and therefore it does not need to be corrected.

The stress amplitudes obtained during cycle counting are corrected to equivalent stress amplitudes at zero mean stress, based on their tensile mean stress values. Various mean stress correction relationships are available for use, such as those shown in Figure 2.4. Two of these have been included in the fatigue script. The Goodman relation, Equation 6.3, is recommended for brittle materials and the Gerber relation, Equation 6.4 is recommended for ductile materials (Suresh, 1991).

$$\sigma_{ac} = \frac{\sigma_a}{1 - \frac{\sigma_m}{S_{UT}}} \tag{6.3}$$

$$\sigma_{ac} = \frac{\sigma_a}{1 - \left(\frac{\sigma_m}{S_{UT}}\right)^2} \tag{6.4}$$

where σ_{ac} is the corrected stress amplitude and S_{UT} is the material ultimate tensile strength.

The use of a mean stress correction method is explained using the Goodman relation as an example. Figure 6.3 shows graphically how the correction is implemented using Equation 6.3. It can be seen that a positive, or tensile, mean stress increases the stress amplitude which in turn causes higher fatigue damage and lowers the fatigue life.

Applying this mean stress correction to a stress history as shown in Figure 6.4(a) results in the corrected history given in Figure 6.4(b). The effect of the mean stress in this case is to double the stress amplitude. The original stress amplitude would likely cause little to no damage being below half the ultimate tensile strength, which is typically the endurance limit for metals. However, the corrected stress amplitude is much more likely to cause damage as it is higher than half the ultimate tensile strength.

The Gerber relation described in Equation 6.4 provides a parobolic curve instead of the straight line provided by the Goodman relation.
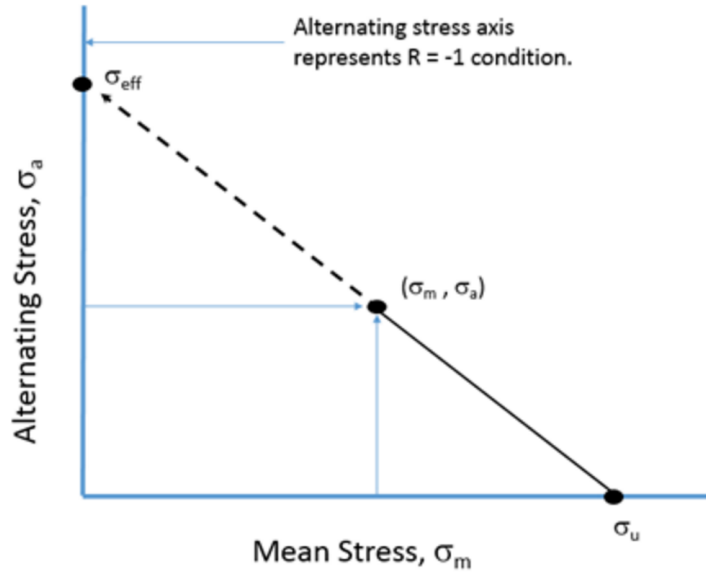
Figure 6.3: Goodman mean stress correction ([Bak, 2016](#))

6.4 Damage accumulation

The fatigue damage is determined using a cumulative damage calculation. The cumulative damage factor is determined using Palmgrin-Miner's linear damage summation rule, presented in Equation 6.5. This rule sums the ratios of cycles experienced at a given corrected stress amplitude (n_i) to cycles needed to fail at that stress amplitude (N_i). When the sum of the ratios (D) is equal to one, the structure is assumed to have failed.

$$\sum_{i=1}^{k} \frac{n_i}{N_i} = D \tag{6.5}$$

The n_i cycles used in Equation 6.5 are determined through cycle counting as described in Section 6.2. The N_i cycles are determined by comparing the stress amplitude to the S-N curve constructed in Section 6.1. The stress amplitudes that are compared to the S-N curve are equivalent Von Mises stresses as recommended by Dowling (2007) and Suresh (1991).

6.5 Validation of the fatigue script

The fatigue script that has been developed is outlined in Figure 6.5. The script has been tested against a study presented by Chen and Wang (1997) in which a roller quenched and tempered RQC-100 steel cantilever beam is subjected to a sudden tip load. The beam is allowed to oscillate to equilibrium and a fatigue analysis is performed on the resulting stress history.
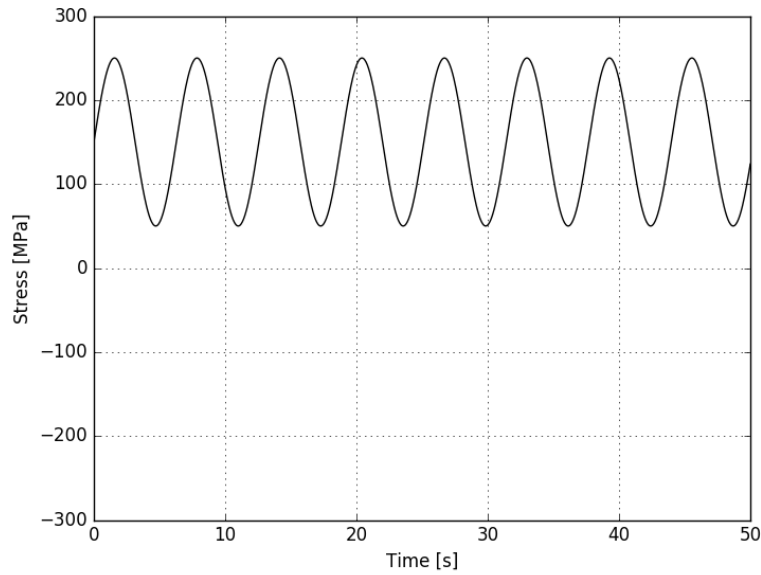
(a) Stress history with $\sigma_a = 100$ MPa, $\sigma_m = 150$ MPa, and $S_{UT} = 300$ MPa
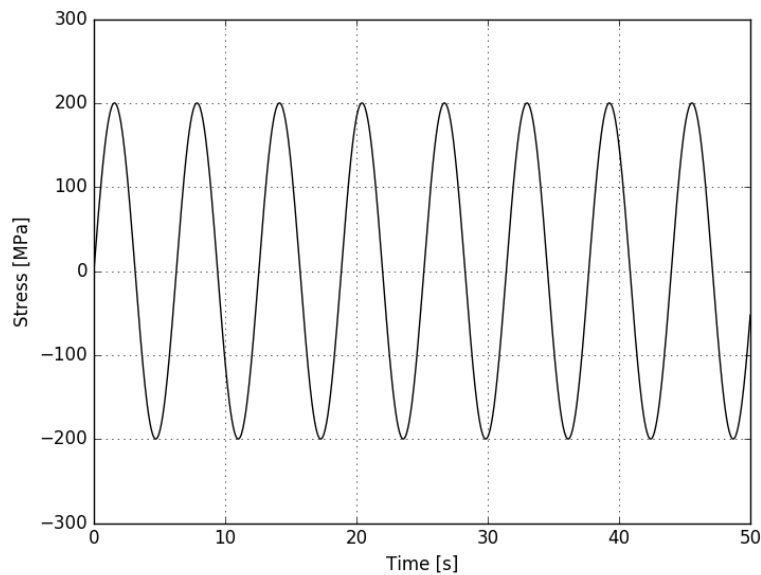
(b) Corrected stress history with $\sigma_{ac} = 200$ MPa

Figure 6.4: Stress amplitude compared with mean stress corrected ampltude

The study was recreated using an FE model of the beam constructed using the MSC Patran/Nastran environment. The stress history at the fixed end of the beam was then exported to the fatigue script. The fatigue life was calculated using a 99% reliability factor for the endurance limit (see Appendix C) on
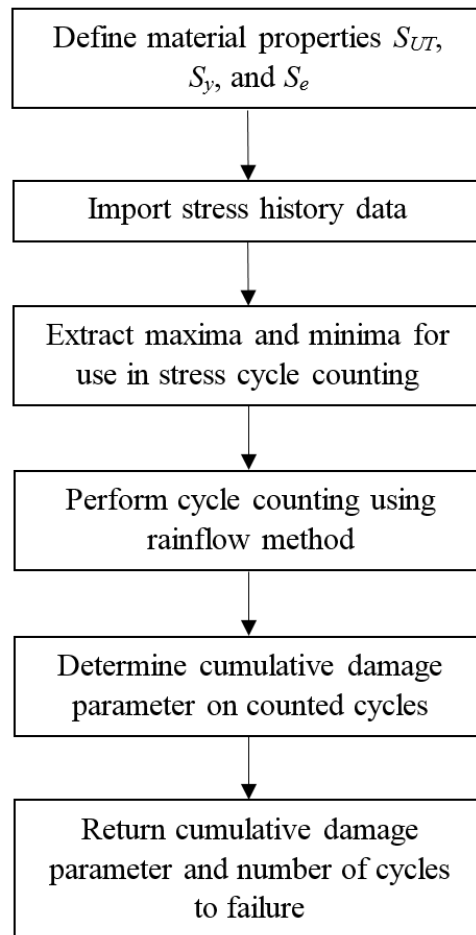
Figure 6.5: Outline of developed fatigue script

the S-N curve. A comparison of the results for a 100 N tip load at a damping ratio of 0.025 is presented in Table 6.1. Included in this table are the analytical results using Euler-Bernoulli beam theory.

The FE model developed for the current study agrees with both the analytical results and with those obtained by Chen and Wang (1997). The results predicted by the developed fatigue script used in the current study show an 11% difference to those of the study done by Chen and Wang (1997). The script is more conservative and the differences in the results can be attributed to the use of an estimated S-N curve rather than the experimentally determined one. It was however necessary to show that this script will work acceptably when using the estimated curve.

In general, it is near impossible to predict fatigue lives to the correct number of cycles. According to Fuchs and Stephens (1980), fatigue lives may vary by as much as a factor of 10 or more for the same material or loading conditions. Researchers in the literature find it acceptable to predict fatigue life to the

Table 6.1: Comparison of results from Chen and Wang (1997) and fatigue script

	Chen and Wang (1997)	Current study	Analytical
Finite element model			
First natural frequency	40.74 Hz	40.74 Hz	40.75 Hz
Second natural frequency	255.29 Hz	255.17 Hz	255.35 Hz
Third natural frequency	714.68 Hz	713.82 Hz	714.98 Hz
Maximum static stress	291.80 MPa	292.00 MPa	291.82 MPa
Maximum displacement	19.32 mm	19.32 mm	19.32 mm
Fatigue			
Damage parameter	5.05e-6	5.66e-6	-
Cycles to failure	198 170	176 575	-

correct order of magnitude and thus the results predicted by the script are satisfactory.

This fatigue script can now be used to analyse the stress history obtained by combining the results of the dynamic model in Chapter 4 and the FE model in Chapter 5. This process is detailed in the following chapter.

Chapter 7

Integration of Numerical Procedures

The FE model, dynamic model, and fatigue script presented in the previous chapters are now integrated to predict the fatigue life of the bogie frame. The results are integrated through use of scripting done in Python v2.7.

The FE model developed in Chapter 5 is used to create result files containing the stress distributions due to unit loads applied at the suspension attachments. Three stress distributions are necessary, one for each load case in the FE model.

The FE results are then read into the script through the use of the pyNastran library (Doyle *et al.*, 2016). This library acts as an interface between Nastran and Python, allowing importing and postprocessing of results within the Python environment.

For each element in the FE model, the equivalent Von Mises stress is extracted. This is done for each of the three unit load cases resulting in three Von Mises stress values per element.

Load histories are then obtained through the use of the dynamic model presented in Chapter 4. The load histories are multiplied by the Von Mises stress values for each element. This process results in three stress histories per element, one for each load case.

Finally, the stress histories for each element are superimposed to obtain the full stress history per element.

The fatigue analysis is conducted through the use of the fatigue script developed in Chapter 6, using the obtained stress histories for each element.

Figure 7.1 summarises the integrated numerical procedure. Results from the integrated numerical procedure are presented and discussed in the following chapter.

FE Model:
- Construct model
- Apply unit load cases
- Export stress results as .op2 files

Dynamic Model:
- Construct model
- Apply wheel/track irregularities
- Export suspension load history results as .csv files

Fatigue Analysis:

Read stress results:
- Read stress results per load case from .op2 files
- Extract equivalent Von Mises stresses for each element per load case

Determine stress histories:
- Read load history results from .csv files
- Multiply Von Mises stresses of each element per load case with corresponding load history
- Superimpose stress histories of load cases for each element

Calculate cumulative damage:
- Perform rainflow cycle counting on each elemental stress history
- Calculate cumulative damage parameter and cycles to failure for each cycle counted elemental stress history

Return Results:
- Write fatigue analysis results to .csv file for post-processing
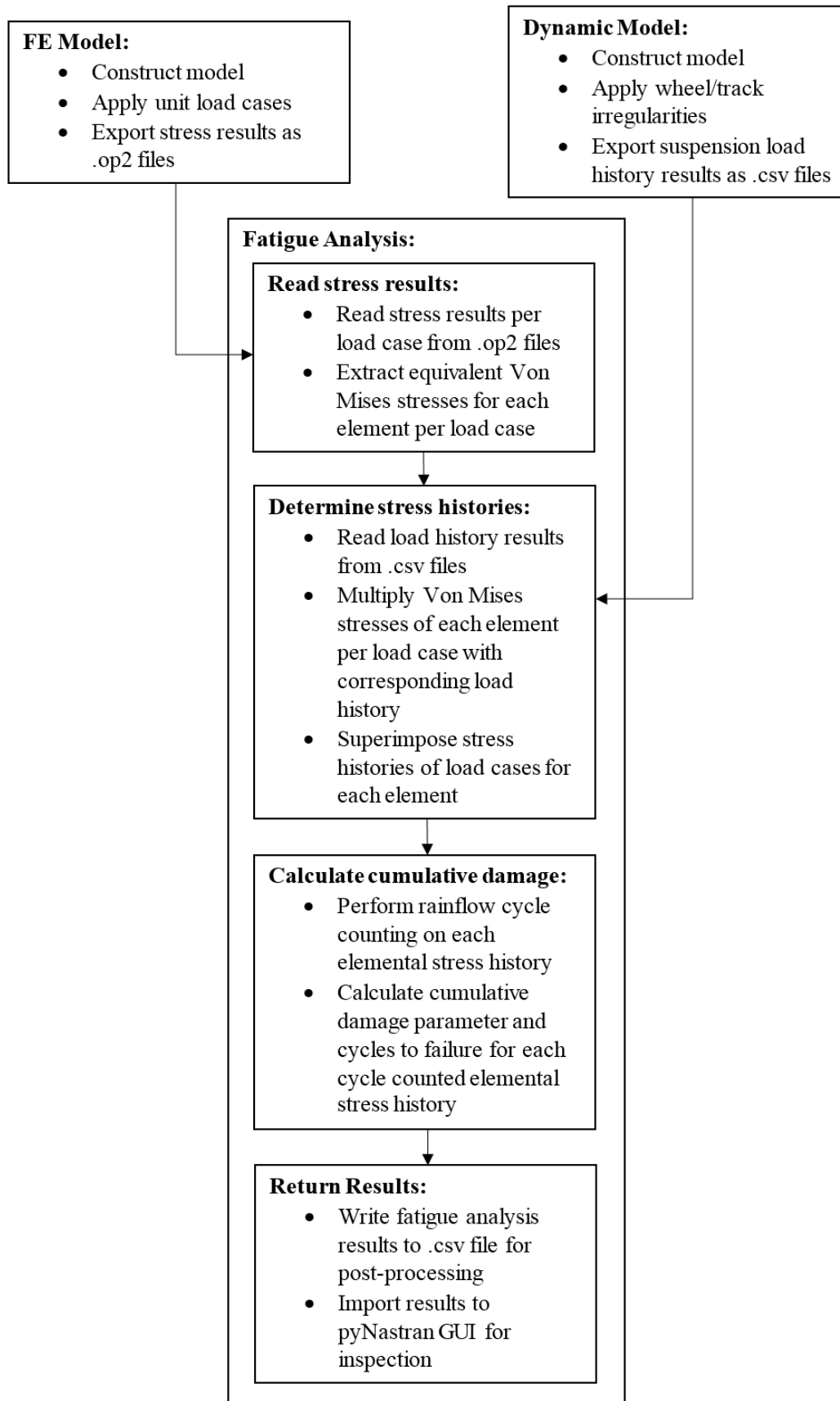- Import results to pyNastran GUI for inspection

Figure 7.1: Summary of integrated numerical procedure

Chapter 8

Results

This chapter presents the results of the numerical processes developed in the previous chapters. The results presented show that the process can be used for the prediction of the fatigue life of the bogie for given parameters. However, further research is required to validate and improve the accuracy of the predictions.

8.1   Simulation parameters

The material properties used for the FE and fatigue simulations are given in Table 8.1. The S-N curve for the fatigue analysis was constructed using a 99% reliability factor on the endurance limit.

The parameters used for the dynamic model were taken from Zhai *et al.* (2001), who provides parameters for both the track and a passenger train such as the class 5M. The bogie and carriage lengths and weights were substituted for those of the class 5M used by Metrorail in South Africa. The loaded mass of the carriage was obtained by adding the mass of the passengers to the tare mass of 30 500 kg. The carriage can hold 160 passengers, and the average body mass in South Africa is reported as 65.6 kg (Walpole *et al.*, 2012). The bogie mass and length were determined from the provided three dimensional model. The parameters are presented in Table 8.2.

Table 8.1: Material properties for FE and fatigue simulation

Property	Value
Modulus of elasticity	200 GPa
Poisson's ratio	0.3
Density	7850 kg/m^3
Yield strength	260 MPa
Ultimate tensile strength	490 MPa

Table 8.2: Parameters for dynamic simulation

Parameter	Symbol	Value
Carriage mass (loaded)	M_c	40 500 kg
Carriage mass moment of inertia	J_c	2.312×10^6 kg.m^2
Bogie mass	M_b	2 000 kg
Bogie mass moment of inertia	J_b	2 200 kg.m^2
Wheelset mass	M_w	1 900 kg
Primary suspension stiffness	K_{s1}	2.312×10^6 N/m
Primary suspension damping	C_{s1}	1.2×10^5 N.s/m
Secondary suspension stiffness	K_{s2}	8.0×10^5 N/m
Secondary suspension damping	C_{s2}	2.174×10^5 N.s/m
Length between bogies	L_c	16 m
Length between bogie wheelsets	L_b	2.75 m
Rail flexural rigidity	EI	6.62×10^6 N.m^2
Rail mass per meter	m_r	60.64 kg/m
Sleeper mass	M_s	118.5 kg
Ballast mass	M_{bl}	739 kg
Railpad stiffness	K_p	1.2×10^8 N/m
Railpad damping	C_p	7.5×10^4
Ballast stiffness	K_{bl}	1.82×10^8 N/m
Ballast damping	C_{bl}	5.88×10^4 N.s/m
Subgrade stiffness	K_{sg}	1.47×10^8 N/m
Subgrade damping	C_{sg}	3.115×10^4 N.s/m
Inter ballast stiffness	K'_{bl}	7.84×10^7 N/m
Inter ballast damping	C'_{bl}	8.0×10^4 N.s/m
Distance between sleepers	L_s	0.545 m
Hertzian contact stiffness	C_H	87.0×10^9 N/m$^{3/2}$

8.2 Dynamic model results

The dynamic model has been simulated using the parameters in Table 8.2 with a train travelling at 50 km/h, 60 km/h, and 80 km/h. A track irregularity in the form of an indentation on the rail surface was included. A small irregularity will likely not cause fatigue failure due to the safety factors inherent in the bogie's design process. The irregularity is therefore exaggerated in order to facilitate the occurrence of fatigue failure. The length and depth of the irregularity were 150 mm and 6 mm respectively.

The contact force at the leading wheelset predicted by the dynamic model is shown in Figure 8.1. It can be seen that as the wheel enters the irregularity at 0.05 seconds that the contact force reduces to zero indicated derailment of the wheelset. Following this is a large impact, the P_1 force, as the wheel makes contact with the rail once again. In the case of Figures 8.1(a) and 8.1(b) multiple instances of derailment occur. It was found that increasing the speed

of the train resulted in a higher P_1 contact force between the wheel and the rail. The contact force however is damped more significantly at higher speeds and there is less chance for multiple derailment.

The contribution of the bogie's trailing wheelset to the contact force at the leading wheelset can also be seen. In the case of Figure 8.1(a), the trailing wheelset hits the irregularity at 0.254 seconds.

The suspension forces are provided in Figure 8.2. It was found that at higher speeds, more energy from the impact was dissipated into the track and through the suspension dampers. This, along with the contact forces being more significantly dampened at high speeds, leads to the suspension forces becoming smaller. Thus, at higher speeds the fatigue damage is reduced for the type of irregularity simulated here. It should be noted that this is not necessarily true in general.

8.3   Fatigue results

The fatigue analysis has been conducted on the bogie FE model using the parameters in Table 8.1 and the results of the dynamic model in Section 8.2. It was found that the bogie fails in the stress hotspots identified in Chapter 5, in the areas where mesh refinements were performed, as depicted in Figure 5.6. Figure 8.3 shows the geometry represented by the solid elements and highlights the hotspot that experienced the highest fatigue damage. This hotspot is located on the inside join between the bogie's leading crossbeam and the sideframe. Figure 8.4 shows the cycles to failure at this hotspot for each speed that was simulated.

In Figure 8.4 the elements are considered not to fail if their life extends past one million cycles. Figure 8.4(a) shows a fatigue failure beginning at 15 552 cycles. In essence, this means the bogie is capable of experiencing the defined irregularity 15 552 times while travelling at 50 km/h before a fatigue failure occurs. It should be noted that due to the unsure nature of fatigue prediction and the assumed parameters used in this study, this number cannot be taken to be exactly accurate. Similarly, Figure 8.4(b) shows that a fatigue failure occurs after 208 200 cycles when the train travels through the irregularity at 60 km/h. At 80 km/h, as seen in Figure 8.4(c), fatigue failure does not occur.

The results achieved here are significantly localised which indicates the possibility of mesh irregularities in this area. As stated in Chapter 5, solid elements were introduced into the FE model specifically to alleviate this problem when it occurred while using only shell elements. Closer inspection of the FE model in this local region reveals that these elements are simply experiencing high stress values under the specified loading conditions and there does not appear to be a stress irregularity caused by the mesh. The localisation of the fatigue failure results could be due to the fact that the element stress values

were used for the fatigue analysis. It is possible that using nodal stress values will provide a better distribution.

It was also noted during post-processing of the fatigue results that failure was occurring at the interface between the solid and shell elements. This was due to artificial stress concentrations imposed on the model by joining the solid and shell elements and were thus ignored for the purpose of fatigue life prediction.

The results presented in this chapter show that the integrated numerical procedure can be used to predict the fatigue life of the Class 5M railway bogie. However, further research is required in order to make more accurate predictions. Recommendations on future research opportunities to better the results achieved with this study are provided in the following chapter.
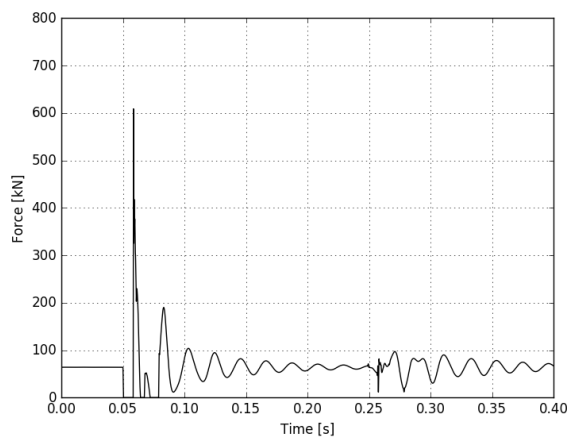
(a) $V = 50$ km/h
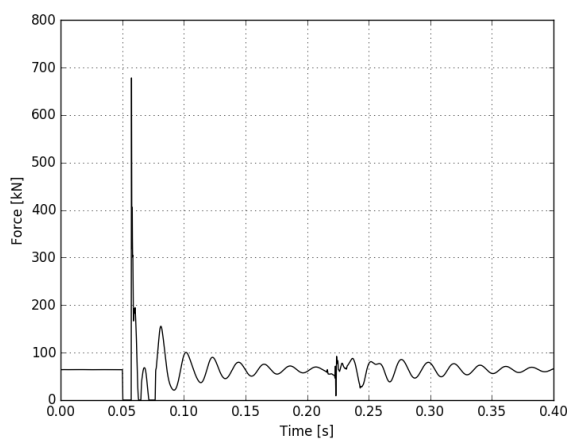
(b) $V = 60$ km/h
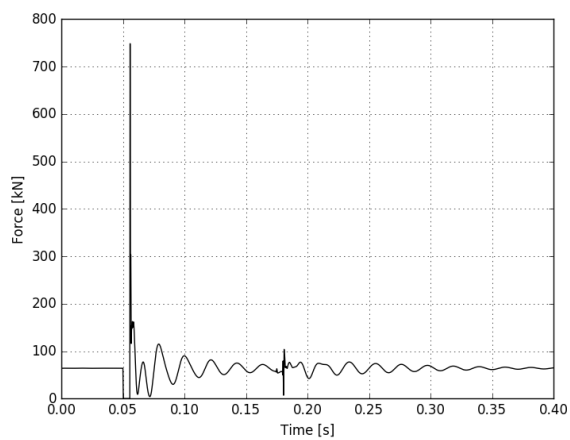
(c) $V = 80$ km/h

Figure 8.1: Contact force for leading wheelset at various speeds
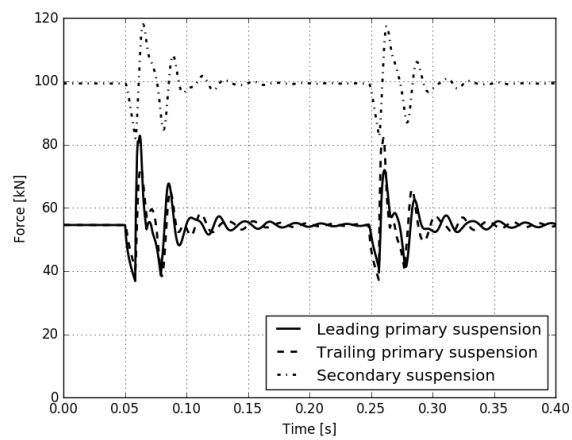
(a) $V = 50$ km/h
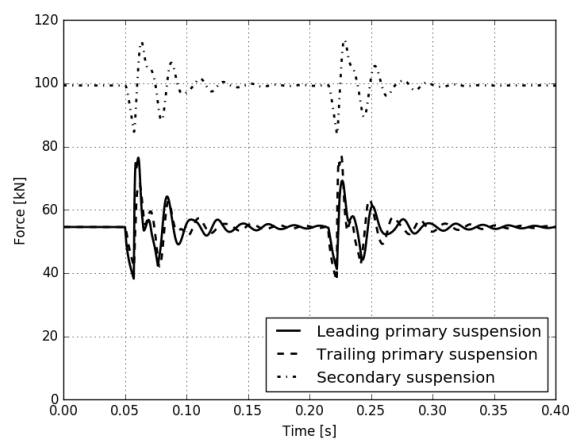
(b) $V = 60$ km/h
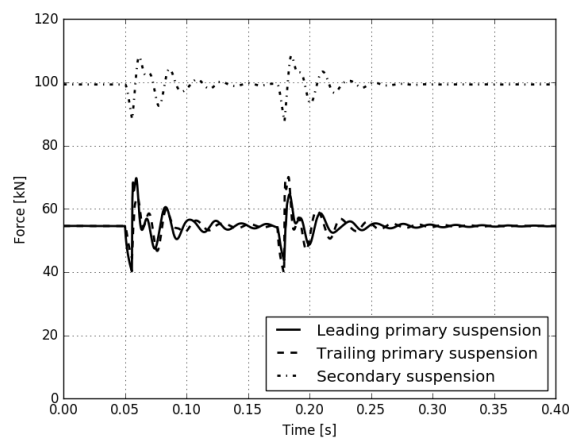
(c) $V = 80$ km/h

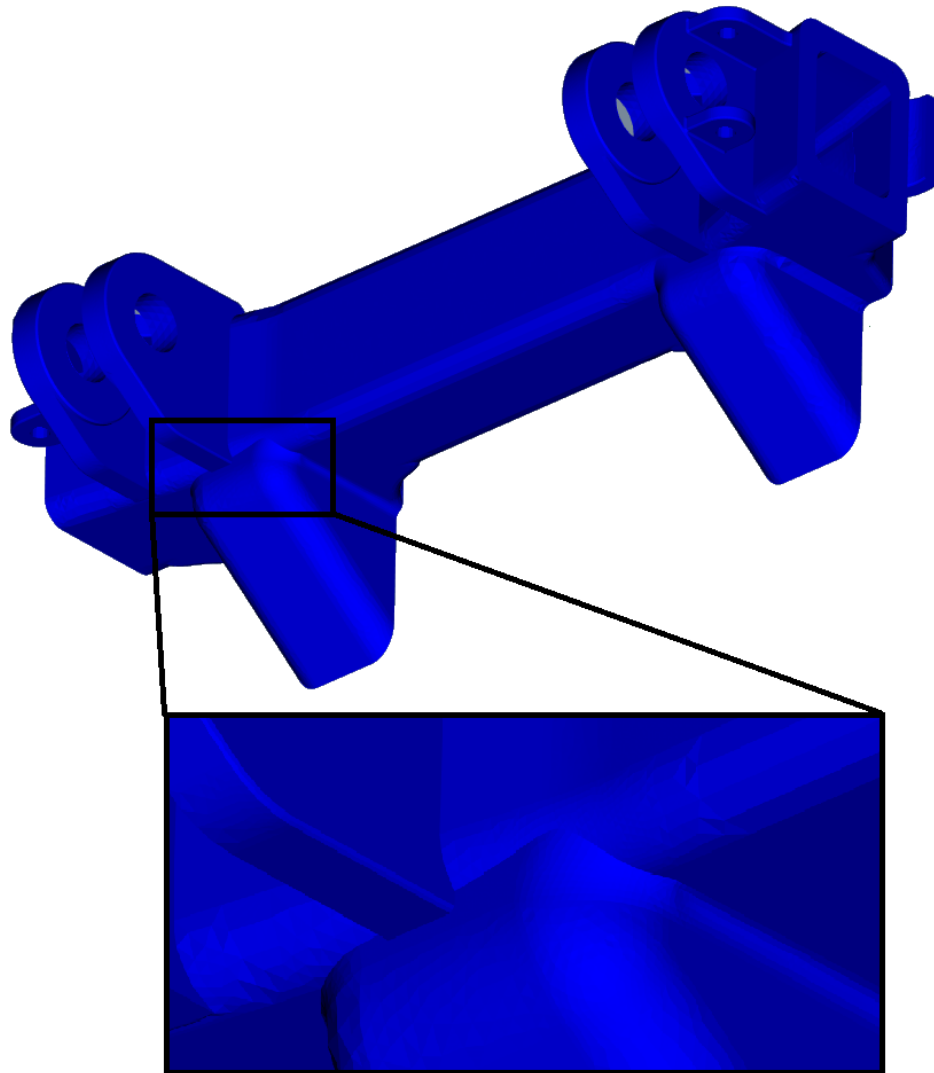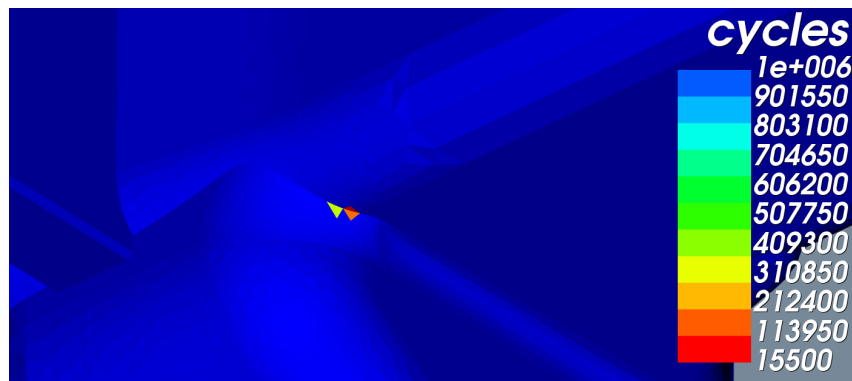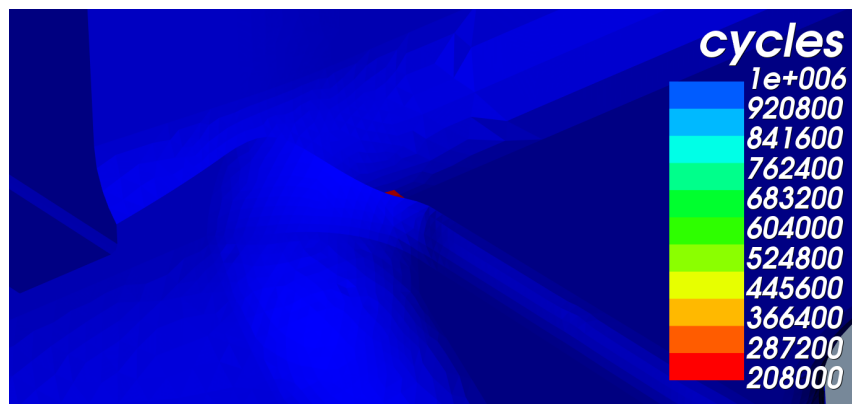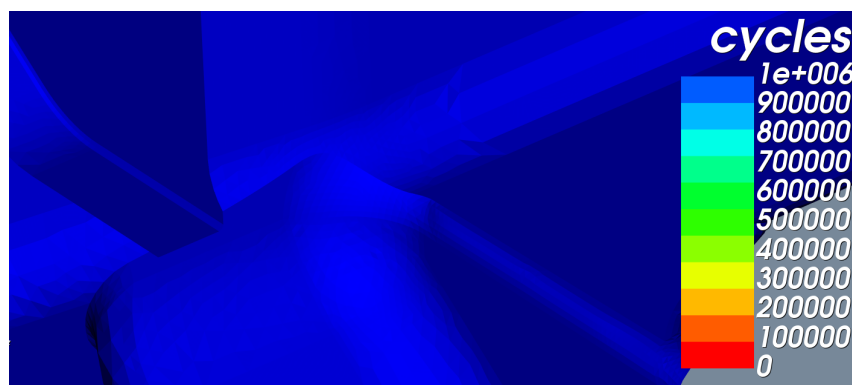**Figure 8.2:** Suspension forces for leading bogie at various speeds

Figure 8.3: Bogie fatigue failure hotspot

(a) $V = 50$ km/h

(b) $V = 60$ km/h

(c) $V = 80$ km/h

Figure 8.4: Cycles to failure for leading bogie at various speeds

Chapter 9

Recommendations and Future Work

This chapter provides recommendations for future research.

9.1   Finite element modelling

This research assumed properties for the FE and fatigue analyses, based on those typical of steel. The bogie is made from BS3100 Grade A2 steel, and greater accuracy could be achieved by determining and using the bogie's actual material properties. This should preferably be done by obtaining test samples from bogies. Furthermore, test samples from a variety of bogies at different stages in their life cycle could be tested to provide data for comparative or statistical studies.

Furthermore, there are more loads present on the bogie than those of the suspensions. The other attached components such as traction motors, the brake rigging, the bolster and more also provide additional forces and stiffness to the bogie frame. The additional effects of these components could be investigated.

9.2   Dynamic modelling

The simulations of the dynamic model developed for this research made use of a number of parameters defined in literature. The results of the model can be made more accurate if parameters more representative of the 5M train and the tracks in South Africa are obtained. This would require extensive experimental work, especially to characterise the track properties.

With regards to the dynamic properties of the train, the spring and damper properties of the suspensions are of primary concern. A prototype compression spring test rig has been designed and was refined by Smith (2016). The

rig can be used to determine the spring properties of the primary and secondary suspension springs. An image of the prototype test rig is provided in Figure 9.1(a). The damper properties can be determined using a load frame capable of applying cyclic loads at various amplitudes and frequencies, such as the MTS load frame shown in Figure 9.1(b) which is available for use at the Department of Mechanical and Mechatronic Engineering at Stellenbosch University. Further investigation is required as to the suitability of the use of this load frame.

(a) Prototype compression spring test rig

(b) MTS load frame

Figure 9.1: Experimental equipment for spring and damper testing

The dynamic simulation can also be conducted through the use of commercial Multi-body Simulation (MBS) software. Packages such as VI-Rail (VI-Grade, 2016), a rail specific add on for MSC Adams, can simulate rail vehicles in a multitude of various operating conditions.

Possible research includes the opportunity of including a bogie FE model as a flexible body within the MBS software. This will then allow the direct calculation of stress due to operating conditions which can be exported for fatigue analysis, or analysed using built in commercial fatigue codes. Due to this an FE model need only be constructed and imported to the MBS software,

with no further FE analysis necessary. The additional components mentioned in Section 9.1 can also easily be added to the bogie model in the MBS software to investigate their effects.

The software also facilitates the creation of predefined tracks or tracks defined using measured data from established railways. This allows the direct simulation of operating conditions of the rail vehicle as experienced in real world applications.

It should be noted that the creation and validation of models using commercial software can be complex. Furthermore, the integration of multiple software environments such as MBS and FE modelling is also not easily done.

Other MBS software with rail simulation capability include SIMPACK (Simulia, 2016), NUCARS (Transportation Technology Centre, Inc, 2016), and VAMPIRE (Resonate Group, Ltd, 2016).

9.3   Fatigue simulation

As stated in Section 9.1, the developed fatigue script makes use of assumed material properties which leads to the use of an estimated S-N curve. The accuracy of the analysis can be increased through experimental determination of the S-N curve for BS3100 Grade A2 steel.

The fatigue script can be expanded to include other fatigue estimation methods such as the strain-life approach, which is more appropriate for low cycle fatigue, or the fracture mechanics approach, which is useful when a fatigue crack has already been identified. Further damage estimation rules can also be included, that are more complex than the linear Palmgrin-Miner rule.

It was noted that the fatigue life results obtained for the bogie were significantly localised. This could be due to the fact that the element stress values were used for the fatigue analysis. The fatigue code could be altered to determine the fatigue life based on the nodal stress results instead of the elemental ones. This will require a considerable amount of postprocessing of the stress results as Nastran does not export the stresses at midside nodes directly. These stresses will need to be interpolated based on the corner node stresses of each element.

Further refinement of the FE model will also likely result in different fatigue life predictions. The sensitivity of the fatigue life prediction with regards to the level of mesh refinement should be investigated in the validation of the process.

9.4   Reliability analysis

The developed numerical procedure can be used to provide statistical data for the fatigue reliability analysis of the bogie.

A possible method to investigate reliability is to use Monte Carlo Simulation (MCS) to produce a hazard function for the expected life of the bogie.

A hazard function can be defined as the rate of change of the conditional probability of failure, given that a system has survived to time t (Singh *et al.*, 2007):

$$h(t) = \lim_{\Delta t \to 0} \frac{R(t) - R(t + \Delta t)}{\Delta t R(t)} = \frac{-R(t)}{R(t)} = \frac{f(t)}{R(t)} \tag{9.1}$$

where $R(t)$ is the reliability function that can be determined based on a probability density function $f(t)$ or a cumulative distribution function $F(t)$, Equation 9.2.

$$R(t) = \int_t^\infty f(t)dt = 1 - F(t) \tag{9.2}$$

Basically a hazard function describes the failure rate of a system, the ratio between the number of failures in time t and number of survivors in time t (Patev, 2015). Most engineering systems have a low failure rate for the majority of their useful lives, with higher failure rates at the beginning and end of their useful lives (Singh *et al.*, 2007). Therefore for most systems, the hazard function will form a bathtub distribution as shown in Figure 9.2.
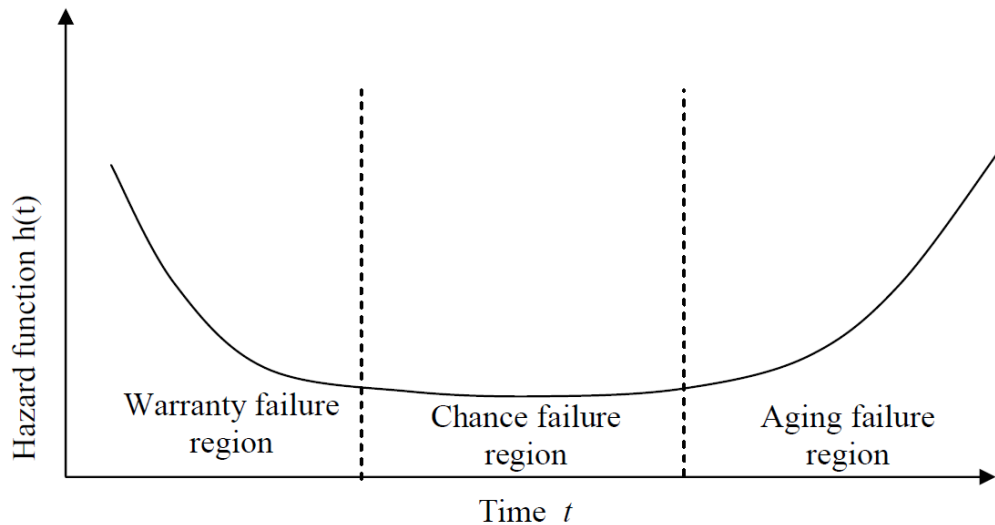
Figure 9.2: Bathtub distribution for hazard function $h(t)$ (Singh *et al.*, 2007)

The dynamic model can be used to generate a database of dynamic load cases that can be used as a domain of possible inputs for the MCS. The loads will be selected randomly based on a probability distribution over the domain. The selected loads can then be used as input for the fatigue analysis to predict the fatigue life for that sample. Furthermore, a statistical material database

can be built up through material testing, and this can form another input for the MCS. This process will have to be repeated to build a database of samples that can be used to accurately predict the reliability of the bogie. The process is summarised in Figure 9.3.

Once the hazard function is constructed, it is a simple matter to predict the reliability of the bogie at any given time in its life cycle.
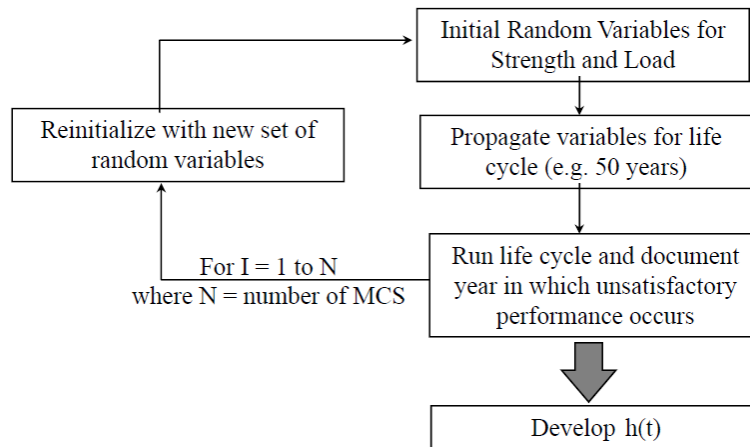

Figure 9.3: Summary of the reliability analysis process, adapted from Patev (2015)

Chapter 10

Conclusion

A numerical process has been successfully designed and implemented to predict the fatigue life of the Class 5M railway bogie. This numerical process includes:

- A model that determines dynamic loads acting on the bogie for some given operating conditions;

- An integrated script that provides the stress histories of the bogie due to the dynamic loads through the use of an FE model and that provides a prediction of the fatigue life of the bogie based on the obtained stress histories.

This process can be useful in the analysis of currently employed or new rolling stock, and can be expanded to analyse other classes of bogies. However, further research is required to validate and improve the accuracy of the predictions provided by the numerical process.

Recommendations to improve the accuracy of the process have been provided, including the testing of material and dynamic properties of components to provide more appropriate results.

Appendices

Appendix A

Rail Vehicle and Track Terminology

The terminology used in this study to describe the rail vehicle and track is presented in this Appendix.

A.1   Vehicle terminology

The terms used to describe the rail vehicle include:

- the carriage,

- the bolster,

- the bogie,

- the equaliser beam,

- the spring plank

- the primary and secondary suspensions,

- and the wheelsets.

The **carriage** represents the load carrying portion of the train, either filled with cargo in the case of a freight train or transporting passengers in the case of a passenger train.

The **bogie** is the chassis that holds the wheelsets, suspension, traction motors, and brake rigging. Typically, a carriage will have two bogies, a leading bogie in the front and a trailing one in the rear. The carriage and bogies can be seen in Figure A.1.

A more detailed computer generated image of the bogie can be seen in Figure A.2. Here the **bolster** can be seen which connects the bogie assembly to the carriage. The **secondary suspension** between the bolster and bogie
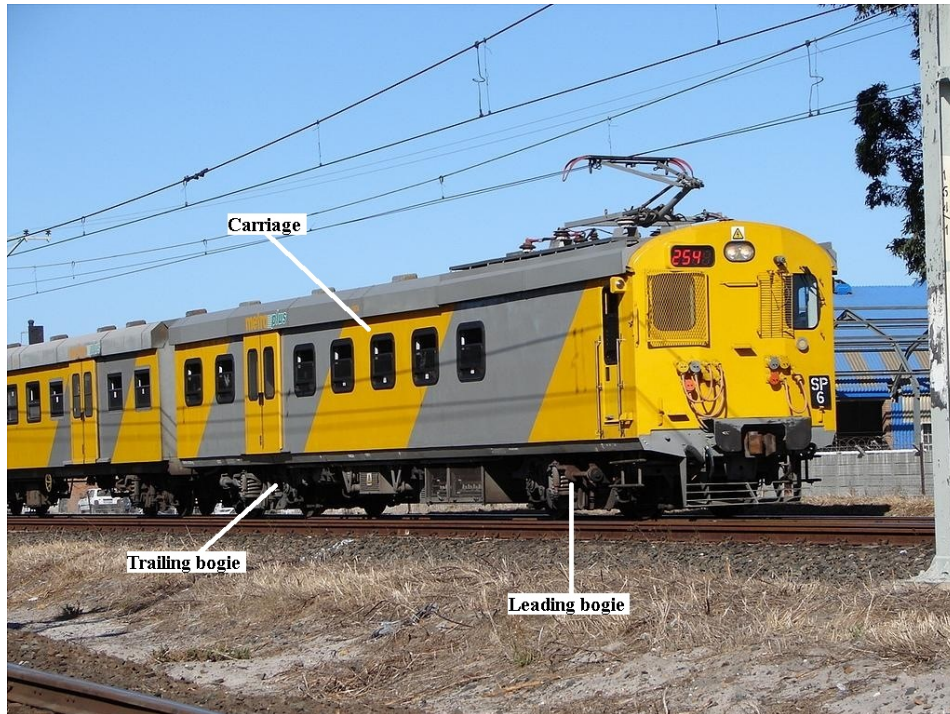
64

Figure A.1: Metrorail 5M2A train (Kritzinger, 2006)

and **primary suspensions** between the bogie and **wheelsets** are also clearly shown.

The load path of the bogie system is summarised in Figure A.3. The vertical forces experienced by the wheel sets is transferred through bearing adaptors to the **equaliser beam**. The load then travels through the primary suspension, a parallel spring-damper system, to the bogie frame. Swing arms then transfer the loads to cross beams placed under the **spring plank**. The loads are then finally passed through the **secondary suspension**, consisting of a set of parallel springs and damper, and onto the **bolster** which transfers the load to the carriage.

A.2 Track Terminology

The terms used to describe, as detailed by Iwnicki (2006) the track include:

- The **rail** of a modern track has a flat bottom with a cross section derived from that of an I-profile. This is also known as a Vignoles profile.

- **Railpads** are placed between the sleepers and rail to help protect the sleepers from wear and impact damage. They also help to electrically insulate the rails.
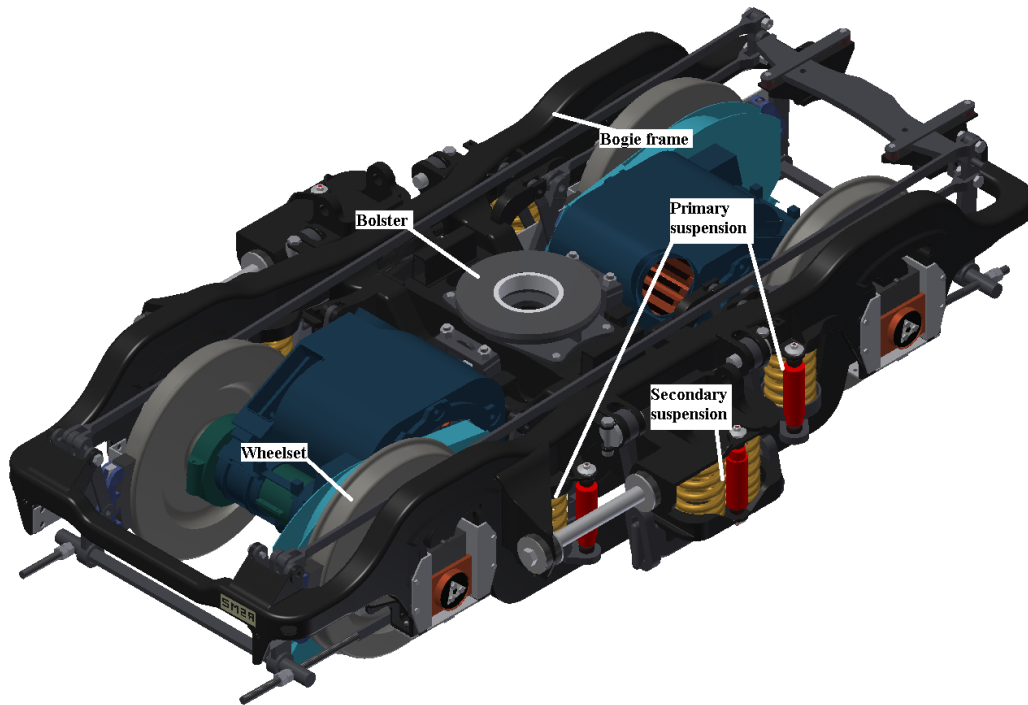
Figure A.2: Metrorail 5M2A bogie
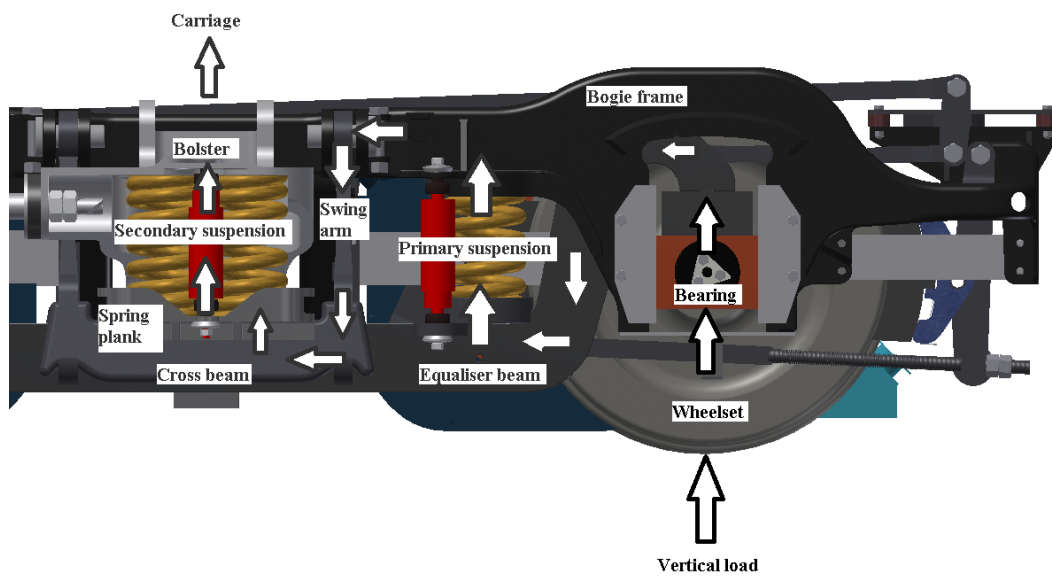
Figure A.3: Load path of the class 5M railway bogie

- The **sleepers** provide discrete support for the rails as well as maintain gauge length (distance between railheads), level, and track alignment.

The sleepers transmit forces form the rail into the ballast. Sleepers can be constructed from concrete, wood, or steel.

- The **ballast** is formed through the use of coarse stones that form a bed. The sleepers are embedded within the ballast, which is tightly compacted around them.

- The **subballast** forms a transitional layer between the ballast and subgrade. It is included to help prevent penetration of the subgrade and ballast.

- The **subgrade** forms the foundation of the track and consists of a levelled surface of earth or rock.

These components are depicted graphically in Figure A.4.

Figure A.4: Cross section of rail track showing its various components (Iwnicki, 2006)

Appendix B
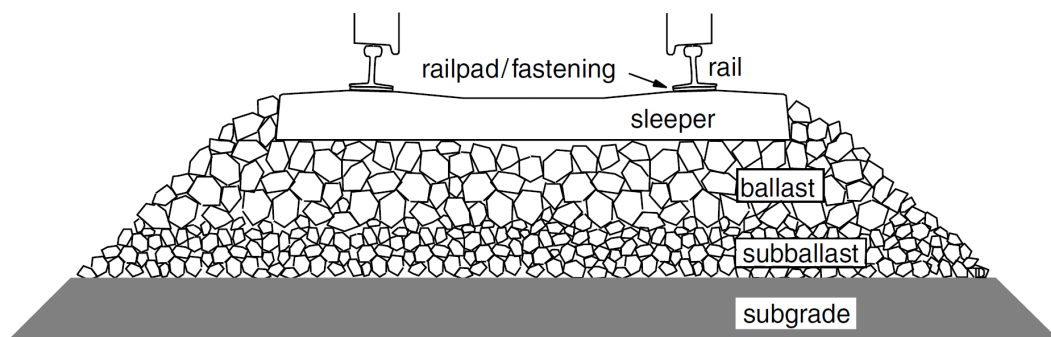
Newmark-β Numerical Integration Scheme

This numerical integration scheme was first presented by Newmark (1959). It has since become a popular solution method for structural dynamics and has been improved and modified by a number of researchers (Wilson, 2002). This method can be used to solve dynamic equations of the form:

$$\mathbf{M}\ddot{\mathbf{x}}_t + \mathbf{C}\dot{\mathbf{x}}_t + \mathbf{K}\mathbf{x}_t = \mathbf{f}_t \tag{B.1}$$

Through direct Taylor series expansion, the following two equations can be derived:

$$\mathbf{x}_t = \mathbf{x}_{t-\Delta t} + \Delta t \dot{\mathbf{x}}_{t-\Delta t} + \frac{\Delta t^2}{2}\ddot{\mathbf{x}}_{t-\Delta t} + \frac{\Delta t^3}{6}\dddot{\mathbf{x}}_{t-\Delta t} + ... \tag{B.2}$$

$$\dot{\mathbf{x}}_t = \dot{\mathbf{x}}_{t-\Delta t} + \Delta t \ddot{\mathbf{x}}_{t-\Delta t} + \frac{\Delta t^2}{2}\dddot{\mathbf{x}}_{t-\Delta t} + ... \tag{B.3}$$

Newmark (1959) provides truncated versions of Equations B.2 and B.3 of the following form:

$$\mathbf{x}_t = \mathbf{x}_{t-\Delta t} + \Delta t \dot{\mathbf{x}}_{t-\Delta t} + \frac{\Delta t^2}{2}\ddot{\mathbf{x}}_{t-\Delta t} + \beta \dddot{\mathbf{x}}_{t-\Delta t} \tag{B.4}$$

$$\dot{\mathbf{x}}_t = \dot{\mathbf{x}}_{t-\Delta t} + \Delta t \ddot{\mathbf{x}}_{t-\Delta t} + \gamma \dddot{\mathbf{x}}_{t-\Delta t} \tag{B.5}$$

where γ and β are truncation constants he introduced.

Furthermore, if the acceleration is assumed as linear across the time step then

$$\dddot{\mathbf{x}}_t = \frac{\ddot{\mathbf{x}}_t - \ddot{\mathbf{x}}_{t-\Delta t}}{\Delta t} \tag{B.6}$$

68

Substituting Equation B.6 into Equations B.4 and B.5 results in Newmark's equations in their standard form:

$$\mathbf{x}_t = \mathbf{x}_{t-\Delta t} + \left(\frac{1}{2} - \beta\right)\Delta t^2\ddot{\mathbf{x}}_{t-\Delta t} + \beta\Delta t^2\ddot{\mathbf{x}}_t \tag{B.7}$$

$$\dot{\mathbf{x}}_t = \dot{\mathbf{x}}_{t-\Delta t} + (1 - \gamma)\Delta t\ddot{\mathbf{x}}_{t-\Delta t} + \gamma\Delta t\ddot{\mathbf{x}}_t \tag{B.8}$$

Equations B.7 and B.8 are then solved by performing an iteration at each time step.

Wilson (1962) reformulated Equations B.7 and B.8 to remove the need for iteration. He proposed rewriting the equations as:

$$\ddot{\mathbf{x}}_t = b_1\left(\mathbf{x}_t - \mathbf{x}_{t-\Delta t}\right) + b_2\dot{\mathbf{x}}_{t-\Delta t} + b_3\ddot{\mathbf{x}}_{t-\Delta t} \tag{B.9}$$

$$\dot{\mathbf{x}}_t = b_4\left(\mathbf{x}_t - \mathbf{x}_{t-\Delta t}\right) + b_5\dot{\mathbf{x}}_{t-\Delta t} + b_6\ddot{\mathbf{x}}_{t-\Delta t} \tag{B.10}$$

where

$$b_1 = \frac{1}{\beta\Delta t^2}$$

$$b_2 = \frac{1}{\beta\Delta t}$$

$$b_3 = \beta - \frac{1}{2}$$

$$b_4 = \gamma\Delta t b_1$$

$$b_5 = 1 + \gamma\Delta t b_2$$

$$b_6 = \Delta t\left(1 + \gamma b_3 - \gamma\right)$$

Equation B.1 can be rewritten, through substitution of Equations B.9 and B.10, in terms of the unknown solution vector for the current time step, Equation B.11. This equation can then be solved directly at each time step.

$$\bar{\mathbf{K}}\mathbf{x}_t = \bar{\mathbf{f}}_t \tag{B.11}$$

where

$$\bar{\mathbf{K}} = \mathbf{K} + b_1\mathbf{M} + b_4\mathbf{C}$$

$$\bar{\mathbf{f}}_t = \mathbf{f}_t + \mathbf{M} \cdot (b_1 \mathbf{x}_{t-\Delta t} - b_2 \dot{\mathbf{x}}_{t-\Delta t} - b_3 \ddot{\mathbf{x}}_{t-\Delta t}) + \mathbf{C} \cdot (b_4 \mathbf{x}_{t-\Delta t} - b_5 \dot{\mathbf{x}}_{t-\Delta t} - b_6 \ddot{\mathbf{x}}_{t-\Delta t})$$

Wilson (2002) shows that this method is unconditionally stable if

$$\frac{1}{2} < \gamma < 2\beta$$

however errors occur if γ is larger than $\frac{1}{2}$.

For the solution of the model presented in this study, the average acceleration assumption is used. This gives $\gamma = \frac{1}{2}$ and $\beta = \frac{1}{4}$. The base code used to implement the integration scheme was provided by Irvine (2012). The code was then altered in order to work with the developed model.

Appendix C

Process for Estimation of Stress-life Curves

A stress-life (S-N) curve provides the relationship between cycles to failure and the applied stress level. An example of an S-N curve is provided in Figure C.1. This appendix provides a method to estimate an S-N curve for a given material based on its material properties.

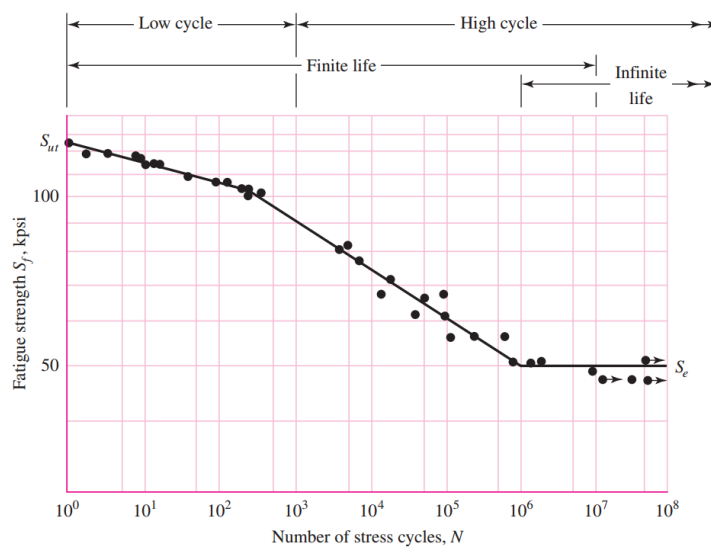**Figure C.1:** Example S-N curve for UNS G41300 steel (Budynas and Nisbett, 2011)

In general, the S-N curve provided for a material has been determined under a fully reversed loading condition. In other words, the mean stress experienced is equal to zero.

In order to construct the estimated S-N curve, it is necessary to define three points. These points exist for steels at $N = 10^0$, $N = 10^3$, and $N = 10^6$.

At $N = 10^0$ the fatigue strength is equal to the ultimate tensile strength of the material (S_{UT}). At $N = 10^3$ the fatigue strength is a factor of S_{UT}, where the factor can be determined using Figure C.2.
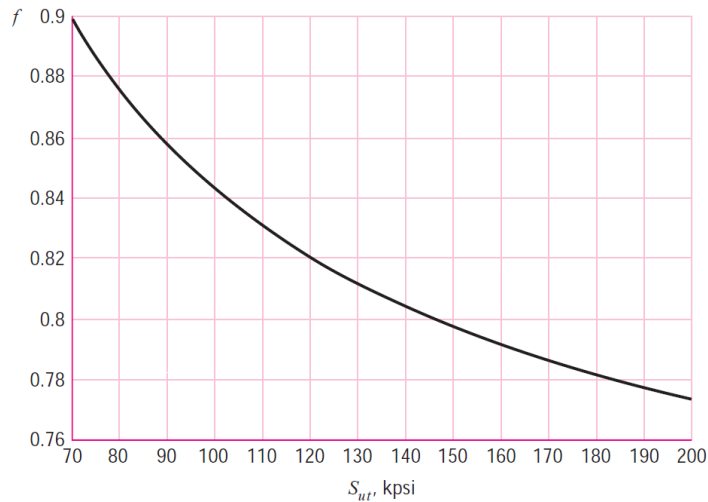

Figure C.2: Fatigue strength fraction for S_{UT} at 10^3 cycles (Budynas and Nisbett, 2011)

At $N = 10^6$ the fatigue strength is equal to the endurance limit for the material. Should the stress amplitude be lower than this limit, the material will theoretically have an infinite life. This limit is assumed to be half of S_{UT} and can be further modified by factors that take into account the size, type of loading, temperature, surface finish, and reliability. The reliability factor is determined through use of Table C.1.

Table C.1: Determination of reliability factor (Budynas and Nisbett, 2011)

Reliability (%)	Reliability factor
50	1.000
90	0.987
95	0.868
99	0.814
99.9	0.753
99.99	0.702
99.999	0.659
99.9999	0.620

Once these three points are known, they are connected using Equation C.1. This equation is defined between two points on the S-N curve.

$$S = aN^b \tag{C.1}$$

where a and b are constants that can be solved using two points on the S-N curve.

Note that this equation will only be valid between the two points it is solved for, hence two equations need be defined for the two regions ($N = 10^0$ - $N = 10^3$ and $N = 10^3$ - $N = 10^6$).

Once these equations are defined, for a given stress level S the number of cycles to failure N can be determined from Equation C.2.

$$N = \left(\frac{S}{a}\right)^{\frac{1}{b}} \tag{C.2}$$

References

Ahlbeck, D.R., Meacham, H.C. and Prause, R.H. (1975). The development of analytical models for railroad track dynamics. *Proceedings of Symposium on Railroad Track Mechanics*, pp. 239–263.

ASTM E1049-85 (2011). *Standard Practices for Cycle Counting in Fatigue Analysis*. West Conshohocken: ASTM International.

Bak, M. (2016). Mean stress corrections in fatigue. https://caeai.com/blog/mean-stress-corrections-fatigue. Accessed: 13 November 2016.

BS EN 13749 (2011). *Railway applications - Wheelsets and Bogies - Methos of specifying the structural requirements of bogie frames*. Brussels: European Committee for Standardization.

Budynas, R.G. and Nisbett, J.K. (2011). *Shigley's Mechanical Engineering Design*. 9th edn. New York: McGraw Hill.

Cera, A., Mancini, G., Leonardi, V. and Bertini, L. (2008). Analysis of methodologies for fatigue calculation for railway bogie frames. *8th World Congress on Railway Research*.

Chen, C. and Wang, I. (1997). Fatigue analysis of a beam subjected to dynamic loading. *15th International Modal Analysis Conference*.

Dietz, S., Netter, H. and Sachau, D. (1998). Fatigue Life Prediction of a Railway Bogie under Dynamic Loads through Simulation. *Vehicle System Dynamics: International Journal of Vehicle Mechanics and Mobility*, vol. 29, no. 6, pp. 385–402. ISSN 0042-3114.

Dowling, N.E. (1971). *Fatigue Failure Predictions for Complicated Stress-strain Histories*. Urbana: Department of Theoretical and Applied Mechanics, University of Illinois.

Dowling, N.E. (2007). *Mechanical Behaviour of Materials: Engineering Methods for Deformation, Fracture, and Fatigue*. 3rd edn. Upper Saddle River: Pearson Prentice Hall.

Doyle, S., Danial, A. and Gasiorek, M. (2016). pyNastran Documentation. https://media.readthedocs.org/pdf/pynastran-git/latest/pynastran-git.pdf. Accessed: 1 November 2016.

Fatemi, A. and Yang, L. (1998). Cumulative fatigue damage and life prediction theories: a survey of the state of the art for homogeneous materials. *International Journal of Fatigue*, vol. 20, no. 1, pp. 9–34. ISSN 0142-1123.

Ferrara, R., Leonardi, G. and Jourdan, F. (2012). Numerical modelling of train induced vibrations. *Social and Behavioural Sciences*, pp. 155–165.

Frost, N.E., Marsh, K.J. and Pook, L.P. (1974). *Metal Fatigue.* London: Oxford University.

Fuchs, H.O. and Stephens, R.I. (1980). *Metal Fatigue in Engineering.* New York: John Wiley & Sons,Inc.

Grassie, S.L., Gregory, R.W., Harrison, D. and Johnson, K.L. (1982). The dynamic response of railway track to high frequency vertical excitation. *Journal Mechanical Engineering Science*, vol. 24, no. 2, pp. 77–90.

Han, J.W., Kim, H.S., Bang, J.S. and Song, S.Y. (2013). Fatigue strength evaluation of bogie frame of urban maglev train with fatigue test on full-scale test rig. *Engineering Failure Analysis*, vol. 31, pp. 412–420. ISSN 1350-6307.

Irvine, T. (2012). Python newmark-beta ode solver. https://vibrationdatapython.wordpress.com/2015/10/09/python-newmark-beta-ode-solver/. Accessed: 25 May 2016.

Iwnicki, S. (2006). *Handbook of Railway Vehicle Dynamics.* Boca Ranton: Taylor & Francis Group.

Johnson, K.L. (1985). *Contact Mechanics.* Cambridge: Cambridge University Press.

Kim, J.S. (2006). Fatigue assessment of tilting bogie frame for Korean tilting train: Analysis and static tests. *Engineering Failure Analysis*, vol. 13, no. 8, pp. 1326–1337. ISSN 1350-6307.

Kritzinger, A. (2006). Metrorail class 5M2A locomotive. http://www.railpictures.net/photo/138642/. Accessed: 25 October 2016.

Lee, Y.-L., Pan, J., Hathaway, R.B. and Barkey, M.E. (2005). *Fatigue Testing and Analysis: Theory and Practice.* Burlington: Elsevier Butterworth-Heinemann.

Li, J., Wang, J., Li, X., Yang, J. and Wang, H. (2015). The Experimental Study for Fatigue Strength of Bogie Frame of Beijing Subway Vehicle Under Overload Situation Bottom View. *The Open Mechanical Engineering Journal*, vol. 9, no. 1, pp. 260–265.

Liao, L. (2011). A study of inertia relief analysis. In: *52nd AIAA/ASME/ASCE/AHS/ASC Structures, Structural Dynamics and Materials Conference.* Denver, Colorado.

Livingstone, C. (2008). Dictionary of sport and exercise science and medicine. http://medical-dictionary.thefreedictionary.com/inverse+dynamics. Accessed: 20 July 2015.

Luo, R.K., Gabbitas, B.L. and Brickle, B.V. (1996). Dynamic Stress Analysis of an Open-shaped Railway Bogie Frame. *Engineering Failure Analysis*, vol. 3, no. 1, pp. 53–64.

Luo, R.K., Gabbitas, B.L., Brickle, B.V. and Wu, W.X. (1998). Fatigue damage evaluation for a railway vehicle bogie using appropriate sampling frequencies. *Vehicle System Dynamics: International Journal of Vehicle Mechanics and Mobility*, vol. 29, no. sup1, pp. 404–415. ISSN 0042-3114.

Mancini, G. and Cera, A. (2006). Design of railway bogies in compliance with new EN 13749 European standard. *7th World Congress on Railway Research.*

Metrorail (2007). Rolling stock. http://www.metrorail.co.za/RollingStock_2.html. Accessed: 16 June 2015.

Mundrey, J.S. (2000). *Railway Track Engineering.* 3rd edn. New Delhi: Tata McGraw Hill.

Newmark, N.M. (1959). A method of computaation for structural dynamics. *ASCE Journal of the Engineering Mechanics Division*, vol. 85, no. EM3.

Newton, S.G. and Clark, R.A. (1979). An investigation into the dynamic effects on the track of wheelflats on railway wagon. *Journal Mechanical Engineering Sciences*, vol. 21, no. 4, pp. 287–297.

Nielsen, J.C.O. and Igeland, A. (1995). Vertical dyanmic interaction between train and track - influence of wheel and track imperfections. *Journal of Sound and Vibration*, vol. 187, no. 5, pp. 825–839.

Oyan, C. (1998). Structural strength analysis of the bogie frame in Taipei rapid transit systems. *Proceedings of the Institution of Mechanical Engineers, Part F: Journal of Rail and Rapid Transit*, vol. 212, no. 3, pp. 253–262. ISSN 0954-4097.

Patev, R.C. (2015). Introduction to engineering reliability. https://www.palisade.com/downloads/pdf/EngineeringReliabilityConcepts.pdf. Accessed: 28 July 2015.

PRASA (2014). Prasa: Corporate plan 2014/15 - presentation to portfolio committee on transport. http://pmg-assets.s3-website-eu-west-1.amazonaws.com/140902prasa.pdf. Accessed: 16 June 2015.

Rangwala, A.S. (2006). *Reciprocating Machinery Dynamics.* New Delhi: New Age International.

Ren, Z., Sun, S., Li, Q. and Liu, Z. (2011). Experimental studies of load characteristics of bogie frames for 350 km/h EMUs. *Proceedings of the Institution of Mechanical Engineers, Part F: Journal of Rail and Rapid Transit*, vol. 226, no. 2, pp. 216–227. ISSN 0954-4097.

Resonate Group, Ltd (2016). VAMPIRE. http://vampire-dynamics.com/simulation/. Accessed: 13 November 2016.

Simulia (2016). SIMPACK Rail. http://www.simpack.com/industrial_sectors_rail.html. Accessed: 13 November 2016.

Singh, V.P., Jain, S.K. and Tyagi, A. (2007). *Risk and Reliability Analysis: A Handbook for Civil and Environmental Engineers*. Reston: American Society of Civil Engineers.

Smith, F.C. (2016). *Test rig for testing train suspension springs*. Stellenbosch University: Department of Mechanical and Mechatronic Engineering.

Stichel, S. and Knothe, K. (1998). Fatigue Life Prediction for an S-Train Bogie. *Vehicle System Dynamics: International Journal of Vehicle Mechanics and Mobility*, vol. 29, no. sup1, pp. 390–403. ISSN 0042-3114.

Sun, Y.Q. and Dhanasekar, M. (2002). A dynamic model for the vertical interaction of the rail track and wagon system. *International Journal of Solids and Structures*, vol. 39, pp. 1337–1359.

Suresh, S. (1991). *Fatigue of Materials*. Cambridge: Cambridge University Press.

Transportation Technology Centre, Inc (2016). NUCARS. http://www.aar.com/nucars/index.html. Accessed: 13 November 2016.

UIC 615-4 (1994). *Motive power units, bogies and running gear bogie frame structure tests*. International Union of Railways.

VI-Grade (2016). VI-Rail. http://www.vi-grade.com/index.php?pagid=rail. Accessed: 13 November 2016.

Walpole, S.C., Prieto-Merino, D., Edwards, P., Cleland, J., Stevens, G. and Roberts, I. (2012). The weight of nations: an estimation of adult human biomass. *BMC Public Health*, vol. 12, no. 439.

Wilson, E.L. (1962). Dynamic response by step-by-step matrix analysis. In: *Proceedings of the Symposium on the Use of Computers in Civil Engineering*. Labortorio Nacional de Engenharia Civil. Lisbon, Portugal.

Wilson, E.L. (2002). *Three-dimensional Static and Dynamic Analysis of Structures*. 3rd edn. Berkeley: Computers and Structures, Inc.

Younesian, D., Solhmirzaei, A. and Gachloo, A. (2009). Fatigue life estimation of MD36 and MD523 bogies based on damage accumulation and random fatigue theory. *Journal of Mechanical Science and Technology*, vol. 23, no. 8, pp. 2149–2156. ISSN 1738-494X.

Zhai, W., Cai, C.B., Wang, Q.C., Lu, Z.W. and Wu, X.S. (2001). Dynamic effects of vehicles on tracks in the case of raising train speeds. *Proceedings of the Institution of Mechanical Engineers, Part F: Journal of Rail and Rapid Transit*, vol. 215, no. March, pp. 125 – 135.

Zhai, W. and Sun, X. (1994). A Detailed Model for Investigating Vertical Interaction between Railway Vehicle and Track. *Vehicle System Dynamics*, vol. 23, no. sup1, pp. 603–615. ISSN 0042-3114.